

1 **Evaluation of global fine-resolution precipitation products and their**  
2 **uncertainty quantification in ensemble discharge simulations**

3

4 **Wei Qi<sup>1,2</sup>, Chi Zhang<sup>1</sup>, Guangtao Fu<sup>2</sup>, Chris Sweetapple<sup>2</sup> and Huicheng Zhou<sup>1</sup>**

5

6 <sup>1</sup> School of Hydraulic Engineering, Dalian University of Technology, Dalian 116024, China

7 <sup>2</sup> Centre for Water Systems, College of Engineering, Mathematics and Physical Sciences,  
8 University of Exeter, North Park Road, Harrison Building, Exeter EX4 4QF, UK

9 Correspondence to: Chi Zhang (czhang@dlut.edu.cn)

10

11 **Abstract**

12

13 The applicability of six fine-resolution precipitation products, including precipitation radar,  
14 infrared, microwave and gauge-based products using different precipitation computation  
15 recipes, is evaluated using statistical and hydrological methods in northeastern China. In  
16 addition, a framework quantifying uncertainty contributions of precipitation products,  
17 hydrological models and their interactions to uncertainties in ensemble discharges is  
18 proposed. The investigated precipitation products are TRMM3B42, TRMM3B42RT,  
19 GLDAS/Noah, APHRODITE, PERSIANN and GSMAP-MVK+. Two hydrological models  
20 of different complexities, i.e., a water and energy budget-based distributed hydrological  
21 model and a physically-based semi-distributed hydrological model, are employed to  
22 investigate the influence of hydrological models on simulated discharges. Results show  
23 APHRODITE has high accuracy at a monthly scale compared with other products, and  
24 GSMAP-MVK+ shows huge advantage and is better than TRMM3B42 in RB, NSE, RMSE,  
25 CC, false alarm ratio and critical success index. These findings could be very useful for

26 validation, refinement and future development of satellite-based products (e.g., NASA Global  
27 Precipitation Measurement). Although large uncertainty exists in heavy precipitation,  
28 hydrological models contribute most of the uncertainty in extreme discharges. Interactions  
29 between precipitation products and hydrological models can have the simialr magnitude of  
30 contribution to discharge uncertainty as the hydrological models. A better precipitation  
31 product does not guarantee a better discharge simulation because of interactions. It is also  
32 found that a good discharge simulation depends on a good coalition of a hydrological model  
33 and a precipitation product, suggesting that, although the satellite-based precipitation  
34 products are not as accurate as the gauge-based product, they could have better performance  
35 in discharge simulations when appropriately combined with hydrological models. This  
36 information is revealed for the first time and very beneficial for precipitation product  
37 applications.

38

## 39 **1 Introduction**

40

41 Knowledge of precipitation plays an important role in the understanding of the water cycle,  
42 and thus in water resources management (Sellers, 1997;Sorooshian et al., 2005;Wang et al.,  
43 2005;Ebert et al., 2007;Buarque et al., 2011;Tapiador et al., 2012;Yong et al., 2012;Gao and  
44 Liu, 2013;Peng et al., 2014a;Peng et al., 2014b). However, precipitation data are not available  
45 in many regions, particularly mountainous districts and rural areas in developing countries.  
46 For example, Northeast China, which plays an important role in food production to support  
47 the country's population and is also an industrial region with many heavy industries,  
48 frequently suffers from drought, posing a threat to regional sustainable development. In such  
49 areas, due to insufficient gauge observations, alternative precipitation data are required for  
50 efficient water resources management.

51

52 In recent years, implementation of gauge-based and remote satellite-based precipitation  
53 products has become popular, particularly for ungauged catchments (Artan et al., 2007;Jiang  
54 et al., 2012;Li et al., 2013;Müller and Thompson, 2013;Maggioni et al., 2013;Xue et al.,  
55 2013;Kneis et al., 2014;Meng et al., 2014;Ochoa et al., 2014). Numerous precipitation  
56 products have been developed to estimate rainfall, for example: Tropical Rainfall Measuring  
57 Mission (TRMM) products (Huffman et al., 2007), Global Land Data Assimilation System  
58 (GLDAS) precipitation products (Kato et al., 2007), Asian Precipitation - Highly-Resolved  
59 Observational Data Integration Towards Evaluation of Water Resources (APHRODITE) (Xie  
60 et al., 2007;Yatagai et al., 2012), Precipitation Estimation from Remotely Sensed Information  
61 using Artificial Neural Networks (PERSIANN) (Sorooshian et al., 2000;Sorooshian et al.,  
62 2002), and Global Satellite Mapping of Precipitation product (GSMAP) (Kubota et al.,  
63 2007;Aonashi et al., 2009).

64

65 There are uncertainties in these products. Several studies have been carried out to analyze the  
66 uncertainty of TRMM in high latitude regions (Yong et al., 2010;Yong et al., 2012;Chen et al.,  
67 2013a;Yong et al., 2014;Zhao and Yatagai, 2014), but studies in northeast China are few.  
68 Evaluation of GLDAS data has generally been limited to the United States and other  
69 observation-rich regions of the world (Kato et al., 2007); assessments and applications in  
70 other regions are rare (Wang et al., 2011;Zhou et al., 2013). The APHRODITE, PERSIANN  
71 and GSMAP products are seldom evaluated in northeast China using basin scale gauge data  
72 (Zhou et al., 2008). Owing to the high heterogeneity of rainfall across a variety of  
73 spatiotemporal scales, the uncertainty characteristics of precipitation products are variable  
74 (Asadullah et al., 2008;Dinku et al., 2008;Nikolopoulos et al., 2010;Pan et al., 2010). Thus, in  
75 northeast China, it is essential to completely evaluate the applicability of these precipitation

76 products. In addition, it is also worth comparing the performance of different precipitation  
77 computation recipes: for example, the artificial neural network function used in PERSIANN,  
78 the histogram matching approach used in TRMM3B42, and the cloud motion vectors used in  
79 GSMAP-MVK+, because the inter-comparison could reveal the strategies that could be used  
80 to obtain more accurate precipitation data.

81

82 Researchers have implemented precipitation products in discharge simulations and reported  
83 discharge uncertainties (Hong et al., 2006;Pan et al., 2010;Serpetzoglou et al., 2010). Also,  
84 many uncertainty analysis approaches have been introduced to quantify the uncertainty  
85 (Beven and Binley, 1992;Freer et al., 1996;Kuczera and Parent, 1998;Beven and Freer,  
86 2001b;Peters et al., 2003;Heidari et al., 2006;Kuczera et al., 2006;Tolson and Shoemaker,  
87 2007;Blasone et al., 2008;Vrugt et al., 2009a;Vrugt et al., 2009b). In these prior approaches,  
88 one of the popular methods is the generalized likelihood uncertainty estimation (GLUE)  
89 technique, introduced by Beven and Binley (1992). This approach outputs probability  
90 distributions of model parameters conditioned on observed data, and the uncertainties in  
91 model inputs are represented by uncertain parameters. Similar to GLUE, Hong et al. (2006)  
92 proposed a Monte Carlo based method to quantify uncertainty in hydrological simulations  
93 using satellite precipitation data, in which flow simulation uncertainty is represented by  
94 ensemble simulation results.

95

96 In addition to individual contributions from hydrological models and precipitation data, the  
97 interactions between precipitation products and hydrological models also contribute to  
98 uncertainty in simulated discharges. However, to the best of our knowledge, the previous  
99 studies have not quantified the respective contributions of precipitation products,  
100 hydrological models and their interactions to the total discharge simulation uncertainty.

101

102 The overall objectives of this paper are: (1) to investigate the applicability of six  
103 fine-resolution precipitation products using both statistical and hydrological evaluation  
104 methods in a small river basin in northeast China; (2) to propose a framework to quantify the  
105 contributions of various uncertainties from precipitation products, hydrological models and  
106 their interactions to uncertainty in simulated discharges. The precipitation products  
107 investigated are TRMM3B42, TRMM3B42RT, GLDAS/Noah (GLDAS\_Noah025SUBP\_3H),  
108 APHRODITE, PERSIANN and GSMAP-MVK+. Two hydrological models of different  
109 complexities - a water and energy budget-based distributed hydrological model (WEB-DHM)  
110 (Wang et al., 2009a;Wang et al., 2009b;Wang et al., 2009c) and a physically-based  
111 semi-distributed hydrological model TOPMODEL (Beven and Kirkby, 1979) - were  
112 employed to investigate the influence of hydrological models on discharge simulations. The  
113 respective uncertainties from precipitation products, hydrological models and the combined  
114 uncertainties from the interactions between products and models are quantified using a global  
115 sensitivity analysis approach, i.e., the analysis of variance approach (ANOVA). A river basin  
116 with a series of 8-year data is used to demonstrate the methodology.

117

118 The paper is organized as follows. Section 2 introduces the study region, precipitation  
119 products, hydrological models and the proposed framework. Section 3 presents the statistical  
120 evaluation results. Hydrological evaluations and the implementation of the proposed  
121 framework are given in section 4. Discussion is given in section 5. Summary and conclusions  
122 are presented in section 6.

123

## 124 **2 Materials and methodology**

### 125 **2.1 Biliu basin**

126

127 Biliu basin (2814 km<sup>2</sup>), located in the coastal region between the China Bohai Sea and the  
128 China Huanghai Sea, covers longitudes 122.29°E to 122.92°E and latitudes 39.54°N to  
129 40.35°N. This basin is characterized by a snow - winter dry - hot summer climate (Koppen  
130 climate classification) and the average annual temperature is 10.6°C. Summer (July to  
131 September) is the major rainy season. There are 11 rainfall stations and one discharge gauge  
132 which have historical data from January 2000 to December 2007. The average elevation is  
133 240 meters. The gauge distribution in Biliu is shown in Fig. 1. The basin slopes vary from 0  
134 to 38 degrees. Land-use data are obtained from the USGS  
135 (<http://edc2.usgs.gov/glcc/glcc.php>). The land-use types have been reclassified to SiB2  
136 land-use types for this study (Sellers et al., 1996). There are six land-use types, with  
137 broadleaf and needle leaf trees and short vegetation being the main types. Soil data are  
138 obtained from the Food and Agriculture Organization (FAO) (2003) Global data product, and  
139 there are two types of soil in the basin: clay loam-luvisols and loam-phaeozems.

140

### 141 **2.2 Precipitation products**

142

143 The selected precipitation products are shown in Table 1. These data are all freely available.  
144 In these selected precipitation products, APHRODITE is wholly based on gauge data;  
145 TRMM3B42 and GLDAS are remote satellite estimation with gauge data corrections; while  
146 others are remote satellite estimation without gauge data corrections. Remote-based  
147 precipitation estimation has many weaknesses, e.g., microwave estimation could miss  
148 convective rainfall and typhoon rain because of its sparse time interval resolution; infrared

149 estimation has a higher time interval resolution, but it cannot penetrate thick clouds. Ground  
150 rain gauge-based interpolation products are limited by interpolation algorithms, gauge density  
151 and gauge data quality (Xie et al., 2007). The details of data sources used in each  
152 precipitation product can be found in Table 1. The detailed introductions of these products are  
153 as follows.

154

155 TRMM is a joint mission between NASA and Japan Aerospace Exploration Agency designed  
156 to monitor and study tropical rainfall (Kummerow et al., 2000; Huffman et al., 2007). Three  
157 instruments - a visible infrared radiometer, a TRMM microwave imager and a precipitation  
158 radar - are employed to obtain accurate precipitation estimation. The TRMM precipitation  
159 radar is the first space-based precipitation radar and operates between 35°N and 35°S.  
160 Outside this band, the microwave imager is used between 40°N and 40°S, and the visible  
161 infrared radiometer data are used between 50°N to 50°S. Usually the precipitation radar is  
162 considered to give the most accurate estimation from satellite, and data from it are often used  
163 for calibration of passive microwave data from other instruments (Ebert et al., 2007). The  
164 post-real-time product used in this study is the TRMM3B42, which utilizes three data sources:  
165 the TRMM combined instrument estimation using data from both TRMM precipitation radar  
166 and the microwave imager; the GPCP monthly rain gauge analysis developed by the Global  
167 Precipitation Climatology Center; and the Climate Assessment and Monitoring System  
168 monthly rain gauge analysis. TRMM3B42 applies an infrared to rain rate relationship using  
169 histogram matching, while TRMM3B42RT merges microwave and infrared precipitation  
170 estimation.

171

172 PERSIANN is a product that, using an artificial neural network function, estimates  
173 precipitation by combining infrared precipitation estimation and the TRMM combined

174 instrument estimation (which assimilates with TRMM precipitation radar and microwave  
175 data). GSMAP-MVK+ uses microwave and infrared precipitation data together and combines  
176 cloud motion vectors to generate fine-resolution precipitation estimation.

177

178 The Global Land Data Assimilation System (GLDAS) project is an extension of the existing  
179 and more mature North American Land Data Assimilation System (Rodell et al., 2004). It  
180 integrates satellite- and ground-based data sets for parameterizing, forcing and constraining a  
181 few offline land surface models for generating optimal fields of land surface states and fluxes.  
182 At present, GLDAS drives four Land Surface Models: Mosaic (Koster and Suarez, 1992),  
183 Noah (Chen et al., 1996;Betts et al., 1997;Koren et al., 1999;Ek, 2003), the Community Land  
184 Model (Dai et al., 2003) and Variable Infiltration Capacity model (Liang et al., 1994). Among  
185 them, the GLDAS/Noah Land Surface Model product (GLDAS\_NOAH025SUBP\_3H) has a  
186 3-h  $0.25^\circ \times 0.25^\circ$  resolution, which is desirable for basin scale research. The GLDAS  
187 precipitation data combine microwave and infrared, and also assimilate gauge observations.

188

### 189 **2.3 Criteria for accuracy assessment**

190

191 Uncertainties of precipitation products are evaluated on the basis of basin-averaged rainfall  
192 observations. Four evaluation criteria are used in rainfall amount error assessment:  
193 correlation coefficient (CC), root mean square error (RMSE), Nash-Sutcliffe coefficient of  
194 efficiency (NSE) and relative bias (RB). These are calculated as follows:

$$195 \quad \text{RMSE} = \left( \frac{\sum_{i=1}^n (X_{pi} - X_{oi})^2}{n} \right)^{\frac{1}{2}} \quad (1)$$



196 
$$\text{NSE} = 1 - \frac{\sum_{i=1}^n (X_{pi} - X_{oi})^2}{\sum_{i=1}^n (X_{oi} - \overline{X_o})^2} \quad (2)$$

197 
$$\text{RB} = \frac{\sum_{i=1}^n X_{pi} - \sum_{i=1}^n X_{oi}}{\sum_{i=1}^n X_{oi}} \times 100\% \quad (3)$$

198 where  $X_{oi}$  represents observed data;  $X_{pi}$  represents estimated data;  $n$  is the total number of data  
 199 points. A perfect fit should have CC and NSE values of one. The lower the RMSE and RB,  
 200 the better the estimation. These comparison criteria have been used by many studies (Ebert et  
 201 al., 2007; Wang et al., 2011; Yong et al., 2012), so they are used in this study.

202

203 Probability distributions by occurrence and volume are also analyzed, which can provide us  
 204 with the information on the frequency and on the product error dependence on precipitation  
 205 intensity (Chen et al., 2013a; Chen et al., 2013b). The critical success index (CSI), probability  
 206 of detection (POD) and false alarm ratio (FAR) are used to quantify the ability of  
 207 precipitation products to detect observed rainfall events. These are defined as follows:

208 
$$\text{CSI} = \frac{H}{H + M + F} \quad (4)$$

209 
$$\text{POD} = \frac{H}{H + M} \quad (5)$$

210 
$$\text{FAR} = \frac{F}{H + F} \quad (6)$$

211 where  $H$  is the total number of hits;  $M$  is the total number of misses;  $F$  is the total number of  
 212 false alarms (Ebert et al., 2007; Su et al., 2008). A perfect detection should have CSI and POD  
 213 values equal to one and a FAR value of zero.

214

## 215 **2.4 Hydrological models and data**

### 216 **2.4.1 WEB-DHM**

217

218 The distributed biosphere hydrological model, WEB-DHM (Wang et al., 2009a;Wang et al.,  
219 2009b;Wang et al., 2009c), was developed by coupling a simple biosphere scheme (Sellers et  
220 al., 1986) with a geomorphology-based hydrological model (Yang, 1998) to describe water,  
221 energy and  $CO_2$  fluxes at a basin scale. WEB-DHM has been used in several evaluations  
222 and applications (Wang et al., 2010a;Wang et al., 2010b;Wang et al., 2012;Shrestha et al.,  
223 2013).

224

225 WEB-DHM input data include precipitation, temperature, downward solar radiation, long  
226 wave radiation, air pressure, wind speed and humidity. With the exception of precipitation, all  
227 input data are obtained from automatic weather stations. There are three automatic weather  
228 stations near Biliu, and observations from these are obtained from the China Meteorological  
229 Data Sharing Service System (downloaded from <http://cdc.cma.gov.cn/home.do>). Hourly  
230 precipitation data are downscaled from daily rain gauge observations using a stochastic  
231 method (Wang et al., 2011). Hourly temperatures are calculated from daily maximum and  
232 minimum temperatures using the TEMP model (Parton and Logan, 1981). The estimated  
233 temperatures are also further evaluated using daily average temperature. Downward solar  
234 radiation is estimated from sunshine duration, temperature and humidity using a hybrid  
235 model (Yang et al., 2006). Long wave radiation is obtained from the GLDAS/Noah (Rodell et  
236 al., 2004). Air pressure is estimated according to altitude (Yang et al., 2006). These  
237 meteorological data are then interpolated to  $300\text{ m} \times 300\text{ m}$  model cells through an  
238 inverse-distance weighting approach. Because of the elevation differences among model cells  
239 and meteorological gauges, the interpolated surface air temperatures are further modified

240 with a lapse rate of 6.5K/km. Gauge rainfall data are also interpolated to 300 m × 300 m  
241 model cells and basin-averaged gauge rainfall data are calculated on the basis of interpolation  
242 results. In addition to the above, the leaf area index and fraction of photosynthetically active  
243 radiation data are obtained from level-4 MODIS global products-MOD11A2. Digital  
244 Elevation Model (DEM) is from the NASA SRTM (Shuttle Radar Topographic Mission) with  
245 a resolution of 30 m × 30 m. We resampled the resolution to 300 m in model calculation to  
246 reduce computation cost, while the model processed finer DEM (30 m grid) to generate  
247 sub-grid parameters (such as hillslope angle and length).

248

#### 249 **2.4.2 TOPMODEL**

250

251 TOPMODEL is a physically-based, variable contributing area model of basin hydrology  
252 which attempts to combine the advantages of a simple lumped parameter model with  
253 distributed effects (Beven and Kirkby, 1979). Fundamental to TOPMODEL's  
254 parameterization are three assumptions: (1) saturated-zone dynamics can be approximated by  
255 successive steady-state representations; (2) hydrological gradients of the saturated zone can  
256 be approximated by the local topographic surface slope; and (3) the transmissivity profile  
257 whose form declines exponentially with increasing vertical depth of the water table or storage  
258 is spatially constant. On the basis of the above mentioned assumptions, the index of  
259 hydrological similarity is represented as the topographic index,  $\ln(a / \tan \beta)$ , for which  $a$   
260 is the area per unit contour length and  $\beta$  is the local slope angle. More detailed descriptions of  
261 TOPMODEL and its mathematical formulation can be found in Beven et al. (1979).  
262 TOPMODEL has been popularly utilized in research across the world (Blazkova and Beven,  
263 1997;Cameron et al., 1999;Hossain and Anagnostou, 2005;Bastola et al., 2008;Gallart et al.,  
264 2008;Bouilloud et al., 2010;Qi et al., 2013), because of its relatively simple model structure.

265 The input data of TOPMODEL mainly includes basin averaged precipitation and topographic  
266 data which can be estimated from DEM.

267

## 268 **2.5 The proposed framework**

269

270 Fig. 2 shows the diagrammatic flowchart of the proposed framework for quantification of  
271 uncertainty contributions to ensemble discharges simulated using precipitation products. This  
272 framework includes four parts: (a) selection of precipitation products; (b) selection of  
273 hydrological models; (c) ensemble discharge simulations using the hydrological models and  
274 precipitation products; and (d) quantification of individual and interactive contributions using  
275 the analysis of variance (ANOVA) approach including contributions from precipitation  
276 products, hydrological models and interactions between models and products. Because the  
277 spatial resolution of selected precipitation products does not correspond with WEB-DHM  
278 model cells, the following procedures were carried out for basin averaged rainfall  
279 calculations: (1) resampling  $0.25^\circ$  or  $0.1^\circ$  precipitation product grids into  $300\text{ m} \times 300\text{ m}$  cells  
280 (the grid size used in WEB-DHM simulations); (2) calculating basin-averaged precipitation  
281 using  $300\text{ m}$  precipitation product grids located within the basin boundary. Diagrammatic  
282 descriptions of these procedures are shown in Fig. 1d. Because WEB-DHM needs hourly  
283 input data, for the 3-hour resolution precipitation products, we assumed rainfall is uniformly  
284 distributed within each 3-hour period. For daily resolution products, we used the same  
285 approach as downscaling observed precipitation data. This downscaling approach may affect  
286 uncertainty in simulated discharge. However, Wang et al. (2011) have already successfully  
287 applied the downscaling approach, and showing that the influence is negligible.

288

289 The total ensemble uncertainty  $Y$  is the variance of discharges. To relate  $Y$  to the uncertainty

290 sources, the superscripts  $j$  and  $k$  in  $Y^{j,k}$  represent a combination of precipitation product  $j$   
 291 and hydrological model  $k$

$$292 \quad Y^{j,k} = P^j + M^k + PM^{j,k} \quad (7)$$

293 where  $P$  represents the effect of  $j$ th precipitation product,  $M$  represents the effect of  $k$ th  
 294 hydrological model, and  $PM$  represents the interaction effect. In this study,  $j$  varies from  
 295 one to six, and  $k$  varies from one to two. Details of the quantification are explained in the  
 296 follow sections.

297

### 298 **2.5.1 Subsampling approach**

299

300 ANOVA could underestimate variance when the sample size is small (Bosshard et al., 2013).  
 301 To reduce the effect of the sample size, Bosshard et al. (2013) proposed a subsampling  
 302 method, which was used in this paper. In the subsampling method, the superscript  $j$  in Eq. (7)  
 303 is replaced with  $\mathbf{g}(h,i)$ . According to Bosshard et al. (2013), in each subsampling iteration  $i$ ,  
 304 data from two products should be selected out of all the six products, and thus 15  
 305 combinations can be obtained. Therefore, the superscript  $\mathbf{g}$  becomes a  $2 \times 15$  matrix:

$$306 \quad \mathbf{g} = \begin{pmatrix} 1 & 1 & \dots & 1 & 2 & 2 & \dots & 4 & 4 & 5 \\ 2 & 3 & \dots & 6 & 3 & 4 & \dots & 5 & 6 & 6 \end{pmatrix} \quad (8)$$

307

### 308 **2.5.2 Uncertainty contribution decomposition**

309

310 Based on the ANOVA theory (Bosshard et al., 2013), total error variance (SST) can be  
 311 divided into sums of squares due to the individual effects as:

$$312 \quad SST = SSA + SSB + SSI \quad (9)$$

313 where  $SSA$  is the error contribution of precipitation products,  $SSB$  is the error contribution of

314 hydrological models and SSI is the error contribution of their interactions.

315

316 The terms can be estimated using the subsampling procedure as follows:

317 
$$\text{SST}_i = \sum_{h=1}^H \sum_{k=1}^K \left( Y^{\mathbf{g}(h,i),k} - Y^{\mathbf{g}(o,i),o} \right)^2 \quad (10)$$

318 
$$\text{SSA}_i = K \cdot \sum_{h=1}^H \left( Y^{\mathbf{g}(h,i),o} - Y^{\mathbf{g}(o,i),o} \right)^2 \quad (11)$$

319 
$$\text{SSB}_i = H \cdot \sum_{k=1}^K \left( Y^{\mathbf{g}(o,i),k} - Y^{\mathbf{g}(o,i),o} \right)^2 \quad (12)$$

320 
$$\text{SSI}_i = \sum_{h=1}^H \sum_{k=1}^K \left( Y^{\mathbf{g}(h,i),k} - Y^{\mathbf{g}(h,i),o} - Y^{\mathbf{g}(o,i),k} + Y^{\mathbf{g}(o,i),o} \right)^2 \quad (13)$$

321 where symbol  $^o$  indicates averaging over a particular index;  $H$  is the number of precipitation  
322 products (six in this study) and  $K$  is the number of hydrological models (two in this study).

323 Then the variation fraction  $\eta^2$  is calculated as follows:

324 
$$\eta_{\text{precipitation}}^2 = \frac{1}{I} \sum_{i=1}^I \frac{\text{SSA}_i}{\text{SST}_i} \quad (14)$$

325 
$$\eta_{\text{model}}^2 = \frac{1}{I} \sum_{i=1}^I \frac{\text{SSB}_i}{\text{SST}_i} \quad (15)$$

326 
$$\eta_{\text{interaction}}^2 = \frac{1}{I} \sum_{i=1}^I \frac{\text{SSI}_i}{\text{SST}_i} \quad (16)$$

327  $\eta^2$  has a value between 0 and 1, which represent 0% and 100% contributions to the overall

328 uncertainty of simulated discharges respectively.  $I$  equals 15 in this study. As shown in Eqs.

329 14-16, the subsampling approach is necessary because it guarantees that every contributor has

330 the same denominator  $I$ . This same denominator makes sure that the inter-comparison among

331 precipitation contribution, model contribution and interaction contribution is free of influence

332 from the sampling number of precipitation products and hydrological models.

333

### 334 **3 Statistical evaluations**

#### 335 **3.1 Daily and monthly scales**

336

337 Comparison of precipitation product data and gauge observations at a daily scale is shown in  
338 Fig. 3. Observations are shown on the *x*-axis and precipitation product data are shown on the  
339 *y*-axis. Four criteria, RMSE, CC, NSE and RB, are also shown. GSMAP-MVK+ is the best  
340 product and PERSIANN has the poorest performance with respect to RMSE and NSE.  
341 GSMAP-MVK+ is also the best with respect to CC, while GLDAS has the poorest  
342 performance with a CC value of 0.55. With respect to RB, APHRODITE performs best and  
343 GSMAP-MVK+ the second best, while TRMM3B42RT the least best with an RB value of  
344 -38%. None of the products can outperform others in terms of all the statistical criteria. This  
345 may be due to the different limitations of satellite sensors and inverse algorithms of  
346 precipitation products. This situation shows that the selection of the best precipitation  
347 products is difficult.

348

349 TRMM3B42RT and TRMM3B42 underestimate precipitation amounts. This underestimation  
350 may be because convective rainfall always happens in summer in northeast China (Shou and  
351 Xu, 2007a, b; Yuan et al., 2010), and indicates the limitation of TRMM algorithms in high  
352 latitude regions with convective rainfall. This type of rainfall has a large rainfall amount  
353 within a short time period and, therefore, cannot be captured by microwave imager. This type  
354 of rainfall may also have a thick cloud that is impenetrable by infrared (Ebert et al., 2007).  
355 Thus microwave and infrared estimation could underestimate rainfall. Compared with  
356 TRMM3B42RT, TRMM3B42 provides an improvement in RB. This improvement may be  
357 attributed to the assimilation with gauge data and histogram matching. Compared with  
358 APHRODITE and GSMAP-MVK+, TRMM3B42 has low accuracy as represented by RB.

359 This implies that the retrieval algorithm used by TRMM3B42 still needs to be improved with  
360 respect to RB. The reason why APHRODITE outperforms TRMM3B42 is that APHRODITE  
361 is a gauge-based product. GSMAP-MVK+ outperforms TRMM3B42 in terms of RB may be  
362 due to the cloud motion vectors it uses. Compared with GSMAP-MVK+, GLDAS/Noah  
363 precipitation shows low accuracy in all the criteria even though they use similar data sources:  
364 IR and MW.

365

366 Comparison of precipitation product data and gauge observations at a monthly scale is shown  
367 in Fig. 4. Here, the APHRODITE product (Fig. 4d) performs best based on RMSE, CC, NSE  
368 and RB. GLDAS/Noah is the poorest in terms of RMSE and NSE. With respect to CC,  
369 GLDAS and TRMM3B42 are equally poor, with CC values of 0.81. The results also show  
370 that PERSIANN overestimates precipitation amount, while Li et al. (2013) found  
371 PERSIANN underestimates rainfall in south China. This may be attributed to the different  
372 latitudes of the study regions.

373

374 Fig. 5 shows time series of average monthly precipitation data against gauge observations  
375 during the period 2000-2007. Each curve represents a different precipitation product. GLDAS  
376 data (Fig. 5a) seriously underestimate high rainfall. Similarly, TRMM3B42RT underestimates  
377 peak precipitation intensity also. Comparatively, APHRODITE, PERSIANN, TRMM3B42  
378 and GSMAP-MVK+ have better performances.

379

### 380 **3.2 Inter-annual evaluations**

381

382 Fig. 6 shows the inter-annual average monthly precipitation. Each curve represents a different  
383 product data. PERSIANN overestimates in all the 12 months, while others underestimate,



384 especially during the summer. This may result from the artificial neural network function and  
385 limitations of infrared and microwave estimation. APHRODITE data are relatively close to  
386 observations. Compared with TRMM3B42RT, TRMM3B42 is better, which indicates the  
387 gauge corrections and histogram matching used by TRMM3B42 impact positively on  
388 accuracy. During the summer, discrepancies between products become larger. With a decrease  
389 of rainfall magnitude, the discrepancies between products reduce. This information implies  
390 that the differences in precipitation estimation algorithms are related to precipitation  
391 magnitudes: the larger the rainfall magnitudes, the greater the differences.

392

### 393 **3.3 Probability distribution evaluations**

394

395 Fig. 7 shows cumulative probability distribution functions (CDF) by occurrence (CDF<sub>c</sub>) and  
396 by volume (CDF<sub>v</sub>) for precipitation products. Probabilities are shown on the y axis, and the x  
397 axis shows rainfall intensity with a 1 mm/day interval log space.

398

399 PERSIANN is the best by both occurrence and volume. However, for CDF<sub>c</sub>, TRMM3B42RT  
400 is the least best, and, for CDF<sub>v</sub>, TRMM3B42RT and GLDAS/Noah are comparable and  
401 worse than others. All precipitation products overestimate occurrence and volume  
402 probabilities except rainfall intensities of larger than 63mm/day and 53mm/day for  
403 occurrence and volume probabilities, respectively. This may be because the precipitation  
404 products overestimate the intensity of some heavy rainfall (recall the results in section 3.1).  
405 The results differ from those of Li et al. (2013), in which PERSIANN has the poorest  
406 performance. This may result from differences in study region (in the study of Li et al. (2013),  
407 south China was studied).

408

### 409 3.4 Contingency statistics

410

411 Fig. 8 shows the false alarm ratio, probability of detection and critical success index for each  
412 precipitation product.

413

414 PERSIANN has the highest false alarm ratio among the products, while TRMM3B42RT has  
415 the lowest. The false alarm ratio of TRMM3B42 is larger than TRMM3B42RT, which  
416 indicates that the gauge corrections and histogram matching used by TRMM3B42 do not  
417 provide positive effects on false alarm ratio and may give rise to uncertainty in false alarm  
418 ratio. GSMAP-MVK+ has a lower false alarm ratio than TRMM3B42.

419

420 No obvious trends are observed for the false alarm ratio overall (compared with the  
421 probability of detection and critical success index), which means the false alarm ratio  
422 dependence on rainfall magnitude is weak. However, Chen et al. (2013a) found the false  
423 alarm ratios of TRMM3B42 and TRMM3B42RT to increase with an increase in rainfall  
424 intensity. The differences are attributed mainly to observed data. In the study of Chen et al.  
425 (2013a), national rain gauge data were employed, whereas in this study more detailed basin  
426 data are used.

427

428 Among all selected products, GLDAS/Noah has the lowest probability of detection and  
429 critical success index during periods of high rainfall intensity, while APHRODITE retains a  
430 high probability of detection and critical success index. This is because APHRODITE uses  
431 gauge observations, and implies that the APHRODITE algorithm is effective. PERSIANN  
432 has comparable probability of detection with APHRODITE. The critical success index of  
433 GSMAP-MVK+ is also comparable with APHRODITE. Compared with TRMM3B42RT,

434 TRMM3B42 has greater probability of detection and comparable critical success index. This  
435 information implies that retrieval algorithm of TRMM3B42 provides positive effects on  
436 probability of detection, but no obvious positive impacts on critical success index.

437

438 Decreasing trends are observed for all products in terms of probability of detection and  
439 critical success index, matching the results of Chen et al. (2013a) for TRMM3B42 and  
440 TRMM3B42RT. This indicates that probability of detection and critical success index have  
441 relatively strong dependence on rainfall magnitude, and implies microwave and infrared  
442 precipitation estimation may have relatively strong dependence on rainfall magnitude in  
443 terms of probability of detection and critical success index.

444

#### 445 **4 Hydrological evaluations**

##### 446 **4.1 Assessment of hydrological models**

447 WEB-DHM was calibrated against observed discharges of Biliu. Six main parameters were  
448 selected to calibrate using a trial and error approach due to the model's computational burden.  
449 Model parameter multipliers were calibrated, similar to the study by Wang et al. (2011). The  
450 'Trial and error' approach has two steps. First, all the multiplier values are set to 1 which  
451 represents the default parameter values from Food and Agriculture Organization (FAO) (2003)  
452 and SiB2 model. Second, varying the multiplier values until acceptable discharge simulation  
453 accuracy is obtained. The calibrated parameter values are listed in Table 2. The simulated  
454 daily, monthly and inter-annual results are shown in Figs. 9a, 9c and 9e.

455

456 TOPMODEL uses basin-averaged parameter values, and these parameter values are estimated  
457 by experience or observation. However, these methods do not give precise parameter values.  
458 Therefore, the parameter values are considered as uncertain and provided with ranges based  
459 on experience (Beven and Kirkby, 1979; Beven and Freer, 2001a, b; Peters et al., 2003). Six

460 parameters of TOPMODEL were calibrated using the dynamically dimensioned search  
461 algorithm (Tolson and Shoemaker, 2007), and the results are given in Table 3. The simulated  
462 daily, monthly and inter-annual results are shown in Figs. 9b, 9d and 9f.

463

464 Note that the parameters of TOPMODEL and WEB-DHM were calibrated using observed  
465 precipitation data, and the accuracy of simulated discharges was validated using gauge  
466 observations. Comparison with the rainfall-runoff model parameter values reported for the  
467 case study catchment in previous research shows the parameter values are appropriate. (Qi et  
468 al., 2013; Qi et al., 2015, 2016).

469

#### 470 **4.2 Daily scale discharges**

471

472 Figs. 10 and 11 display scatterplots of discharges during the period 2000-2007 simulated  
473 using WEB-DHM and TOPMODEL against gauge observations at a daily scale. Two criteria,  
474 NSE and RB, are shown. It should be noted that the start dates are different for  
475 precipitation products, and observed data were used when product data are not available:  
476 from 1 January 2000 to 29 February 2000 for TRMM3B42RT, GSMAP-MVK+ and  
477 PERSIANN; from 1 January 2000 to 23 February 2000 for GLDAS/Noah. These time  
478 periods were not considered for accuracy comparison.

479

480 In the case of WEB-DHM simulations, the best NSE (0.41) corresponds with APHRODITE  
481 (Fig. 10d), while the best value for RB (1%) corresponds with GLDAS/Noah. In the case of  
482 TOPMODEL simulations, the best NSE (0.41) corresponds with APHRODITE, and the best  
483 value for RB (-24%) corresponds with APHRODITE also. Although the best NSE is the same  
484 for both WEB-DHM and TOPMODEL simulations and corresponding product is also the

485 same, there is a large difference in the best RB values. At the daily scale precipitation amount  
486 evaluation, the least best RB is -38%, corresponding with TRMM3B42RT (Fig. 3c). However,  
487 in WEB-DHM discharge simulation, the least best RB (218%) corresponds with PERSIANN,  
488 and, in TOPMODEL simulation, the least best RB (-62%) corresponds with TRMM3B42RT.  
489 These differences stem from differences in hydrological models and interactions between  
490 hydrological models and precipitation product data.

491

492 All RB criteria at the daily scale precipitation evaluations (recall the results in Fig. 3) are  
493 amplified by TOPMODEL, while in the case of WBE-DHM, some are amplified and the  
494 others are decreased. For example, for GLDAS and PERSIANN, the RB criteria at the daily  
495 scale precipitation evaluations are -27% and 28%, but they are -50% and 31% in  
496 TOPMODEL simulations; they are 1% and 218% in WEB-DHM simulations. These  
497 differences result from the influence of hydrological models and interactions between  
498 precipitation products and hydrological models. These results reveal that a hydrological  
499 model can amplify uncertainties in input data but also reduce uncertainties, which may be due  
500 to the nonlinear runoff generation process in hydrological models. This finding is consistent  
501 with the research by Yong et al. (2010).

502

### 503 **4.3 Monthly scale discharges**

504

505 Figs. 12 and 13 display scatterplots of discharges during the period 2000-2007 simulated  
506 using WEB-DHM and TOPMODEL against gauge observations at a monthly scale.

507

508 In the case of WEB-DHM, the best NSE and RB values are 0.73 and 1%, which  
509 corresponding with TRMM3B42 and GLDAS respectively. In the case of TOPMODEL, they

510 are 0.58 and -24%, corresponding with PERSIANN and APHRODITE respectively. The  
511 combination of WEB-DHM and TRMM3B42 shows a satisfactory performance, with NSE  
512 and RB values of up to 0.73 and -7%, even though TRMM3B42 is not the best in monthly  
513 scale precipitation data evaluation. This reveals the influence of different combinations of  
514 hydrological models and precipitation data on discharge simulation, implying that accurate  
515 discharge simulation does not solely depend on the accuracy of a precipitation product.

516

517 At the monthly scale, although APHRODITE is the best precipitation product and  
518 WEB-DHM model has better performance than TOPMODEL in calibration (Figs. 9c and 9d),  
519 the combination of APHRODITE and WEB-DHM is not better in the discharge simulation,  
520 which can be shown by comparing Fig. 12d with Fig. 13d (the RB and NSE of WEB-DHM  
521 and APHRODITE combination are -37% and 0.5, but they are -24% and 0.51 for the  
522 combination of TOPMODEL and APHRODITE). This could be due to the interactive  
523 influence between hydrological models and precipitation products, and implies that the  
524 interactions between models and products could be large and have a big influence on  
525 discharge simulations. In addition, comparison of Figs. 12d and 12b shows that discharge  
526 simulation of APHRODITE is worse than TRMM3B42, even though APHRODITE is the  
527 best precipitation product in terms of all the selected criteria at a monthly scale precipitation  
528 amount evaluation. This information shows that better precipitation products do not guarantee  
529 better discharge simulations. These results imply that, although the satellite-based  
530 precipitation products are not as accurate as gauge-based products in rainfall amount  
531 estimation, they could have a better performance in discharge simulations if the combination  
532 of precipitation product and hydrological model is good.

533

#### 534 **4.4 Inter-annual average monthly discharges**

535

536 Fig. 14 shows inter-annual average monthly discharges of all selected precipitation products  
537 during the period 2000-2007. In the case of TOPMODEL, PERSIANN agrees well with  
538 gauge observations, and all products underestimate discharges in August. In the case of  
539 WEB-DHM, GLDAS data and TRMM3B42 data have a better performance than other data  
540 but, with the exception of PERSIANN, all products underestimate peak discharge in August.  
541 The simulation results show huge differences even though Figs. 9e and 9f show TOPMODEL  
542 and WEB-DHM have almost the same performance using observed data; this is because of  
543 the impacts of interactive influence between hydrological models and precipitation products.

544

#### 545 **4.5 Uncertainty source quantification**

546

547 All above results suggest that discharge simulations are influenced by precipitation products,  
548 hydrological models and interactions between hydrological models and precipitation products.  
549 Thus it is essential to quantify the respective influence. Figs. 15a and 15b show contributions  
550 of precipitation products, hydrological models and their interactions to uncertainties in  
551 monthly average discharges and different flow quantiles respectively. Fig. 15b shows  
552 quantiles computed at a daily time step. The contributions of uncertainty sources are  
553 represented by stripes.

554

555 Fig. 15a shows that precipitation data contribute most of the uncertainty in discharges, and  
556 contribute more than hydrological models. Interactions between hydrological models and  
557 precipitation products have large contributions, at a similar level to those from hydrological  
558 models. In summer (July to September), the contribution of precipitation data is less than

559 most other months except March. However, the uncertainty in precipitation intensity  
560 increases in summer (recall the results in section 3.2). In non-summer months except March,  
561 the uncertainty contribution from precipitation products is larger than in summer. These  
562 differences maybe result from the nonlinear propagation of uncertainty through hydrological  
563 models. In March, the contribution of hydrological models is larger than in other months,  
564 which may result from the decrease in influences of interactions and precipitation products,  
565 and from the nonlinear influence of the hydrological models.

566

567 Fig. 15b shows that, for small discharges (smaller than 25% quantile which corresponds to an  
568 observed discharge value of  $1.79\text{m}^3/\text{s}$ ) and large discharges (larger than 99% quantile which  
569 corresponds to an observed discharge value of  $157\text{m}^3/\text{s}$ ), hydrological models contribute most  
570 of the uncertainties. For middle magnitude flows (between 25% and 99% quantiles),  
571 precipitation products contribute the majority, and the contribution of interactions is not  
572 negligible and of similar magnitude to the contribution from hydrological models. The  
573 contribution of interactions is larger for middle magnitude flows than for small and large  
574 discharges. The different contributions of interactions for various magnitude flows may be  
575 because different magnitude rainfall data could trigger different hydrological processes  
576 (Herman et al., 2013). Small discharges mainly come from base flows which are relatively  
577 stable and do not need much rainfall to be triggered, and large discharges are mainly  
578 controlled by overland flows when heavy precipitation occurs. Middle magnitude discharges  
579 consist of contributions from base flows, lateral subsurface flows and overland flows, and can  
580 be triggered by rainfalls of various magnitudes - thus interactions are more variable.

581

582 Although heavy rainfall data have high uncertainty (recall the results in section 3.1),  
583 precipitation products have a small contribution to uncertainty in large discharges (Fig. 15b).



584 This implies that the uncertainty in high precipitation is compensated by the high nonlinearity  
585 in hydrological models.

586

587 In this study, because hydrological model parameters were calibrated using gauge  
588 observations, the hydrological model parameter uncertainty was not considered. Although the  
589 uncertainty contribution results in this study may not be transferable to other basins, the  
590 proposed framework provides a useful tool for quantifying uncertainty contributions in  
591 discharge simulations using precipitation products.

592

## 593 **5 Discussion**

594 The spatial variations in precipitation are not considered in this study. The study region is a  
595 small river basin, as shown in Fig. 1, there are only 11 grids inside the basin boundary for the  
596 precipitation products with a spatial resolution of 0.25 degree. Within a grid of 0.25 degree,  
597 there are no differences in precipitation amount between the 300 m × 300 m grids used in  
598 hydrological models, and differences exist at the level of 0.25 degree grids only.  
599 Sapriza-Azuri et al. (2015) suggested that the spatial variability of precipitation has little  
600 influence on rapidly responding river discharges; this study is the case because the flow  
601 transport time from the most upper part of the basin to the downstream discharge gauge is 6  
602 hours, which is shorter than the daily and monthly time steps of discharges investigated.  
603 Therefore, the spatial distributions of precipitation products with a resolution of 0.25 degree  
604 in the relatively small river basin have little influence on the simulated discharges. However,  
605 the assumption of uniform distribution can be regarded as another uncertainty source against  
606 spatial variability, and its influence can be assessed using the proposed uncertainty  
607 quantification framework. This will allow us to compare the relative contributions of the  
608 assumption to those from other sources such as hydrological models, which will be

609 investigated using a much larger river basin in future work.

610

611 In addition to improving the accuracy of precipitation products, a good coalition could help to  
612 achieve the performance in discharge simulations. Our approach provides a way to assess the  
613 different coalitions, i.e., the overall uncertainties in simulated discharges from different  
614 combinations of hydrological models and precipitation products. More precipitation products  
615 and hydrological models should be included and tested in future work.

616

617 It should be noted that other input data including temperature, downward solar radiation, long  
618 wave radiation, air pressure, wind speed and humidity may also have uncertainties. However,  
619 Fig. 9 shows that the simulated discharge data are acceptable particularly at monthly and  
620 inter-annual scales using these data. Research has shown that the land surface temperatures  
621 are highly accurate compared with MODIS satellite land surface temperature observations  
622 (Wang et al., 2011; Qi et al., 2015). Thus, the uncertainties from the other inputs are not  
623 considered in our case study river basin.

624

625 In this study, the parameter values calibrated using gauge observations are not tuned to a  
626 specific product. That is, there is little compensation by model parameters for the errors in  
627 input precipitation data. The differences in modeling accuracy mainly results from the  
628 different representations of hydrological processes. That is, the errors in precipitation  
629 products are primarily compensated by the different representations of model processes.

630

## 631 **6 Summary and conclusions**

632

633 This research assesses the applicability of six precipitation products with fine spatial and

634 temporal resolutions at a high latitude region in northeast China using both statistical and  
635 hydrological evaluation methods at multi-temporal scales. A framework is proposed to  
636 quantify uncertainty contributions of precipitation products, hydrological models and their  
637 interactions to simulated discharges. These products are TRMM version 7 products  
638 (TRMM3B42 and TRMM3B42RT), GLDAS, APHRODITE, PERSIANN and  
639 GSMAP-MVK+. The fully distributed WEB-DHM and semi-distributed TOPMODEL were  
640 employed to investigate the influence of hydrological models on simulated discharges. The  
641 results show the uncertainty characteristics of the six products, and reveal strategies that  
642 could improve precipitation products. This information could provide references for future  
643 precipitation product development. The proposed framework can reveal hydrological  
644 simulation uncertainties using precipitation products: thus provides useful information on  
645 precipitation product applications. The following conclusions are presented on the basis of  
646 this study.

647

648 First, at daily scale, selecting the best precipitation products is very difficult, while, at a  
649 monthly scale, APHRODITE has the best performance in terms of NSE, RB, RMSE, and CC,  
650 and also retains a high probability of detection and critical success index. This information  
651 implies that the APHRODITE algorithm is effective, and APHRODITE could be a very good  
652 data set to refine and validate satellite-based precipitation products.

653

654 Second, GSMAP-MVK+ show huge advantage, and is better than TRMM3B42 in RB, NSE,  
655 RMSE, CC, false alarm ratio and critical success index, while PERSIANN is better than  
656 TRMM3B42 in probability of detection and precipitation probability distribution estimation.  
657 At present, the NASA Global Precipitation Measurement (GPM) mission combines the  
658 artificial neural network function of PERSIANN and precipitation radar-matching of TRMM

659 Multi-satellite Precipitation Analysis. However, the above finding implies that incorporating  
660 GSMAP-MVK+ estimation approach into GPM could be useful as well.

661

662 Third, it is found that, although high uncertainty exists in heavy rainfall, hydrological models  
663 contribute mostly to the uncertainty in extreme discharges. This may result from the  
664 nonlinear propagation of uncertainty through hydrological models enlarges the influence of  
665 hydrological models, and implies that high uncertainties in extreme rainfall do not mean high  
666 uncertainties in extreme discharges.

667

668 Fourth, interactions between hydrological models and precipitation products contribute a lot  
669 to uncertainty in discharge simulations, and interactive impacts are influenced by discharge  
670 magnitude. Because of interactive effects, for hydrological models with similar performances  
671 in calibration, using the same precipitation products for discharge simulations does not  
672 provide a similar level of accuracy in discharge simulations, and in fact very different  
673 predictions could be obtained. In addition, this finding implies that only considering  
674 precipitation products or hydrological model uncertainties could result in overestimation of  
675 precipitation product contribution and hydrological model contribution to discharge  
676 uncertainty.

677

678 Fifth, a good discharge simulation depends on a good coalition of a hydrological model and a  
679 precipitation product, and a better precipitation product does not necessarily guarantee a  
680 better discharge simulation. This suggests that, although the satellite-based precipitation  
681 products are not as accurate as the gauge-based product, they could have better performance  
682 in discharge simulations when appropriately combined with hydrological models. It should be  
683 noted that this finding should be further tested with more river basins, in particular large river

684 basins accounting for spatial variability in precipitation products.

685

686 In the future, calculating deterministic discharge simulations considering precipitation  
687 product uncertainties and hydrological model uncertainties together should be studied  
688 because above results show product uncertainties and model uncertainties all are important.  
689 In addition, recalibrating hydrological models using precipitation products may reduce the  
690 interactive influence between hydrological models and precipitation products on simulated  
691 discharges, and this may explain why recalibration can improve discharge simulation  
692 accuracy. This should be verified in future work. Further, future research is encouraged to  
693 incorporate GSMAP-MVK+ estimation approach into GPM because of the good performance  
694 of GSMAP-MVK+.

695

#### 696 **Acknowledgements:**

697

698 This study was supported by the National Natural Science Foundation of China (Grant No.  
699 51320105010 and 51279021). The first author gratefully acknowledges the financial support  
700 provided by the China Scholarship Council. The APHRODITE data were downloaded from  
701 <http://www.chikyu.ac.jp/precip/products/index.html>. The TRMM 3B42 data are downloaded  
702 from [http://mirador.gsfc.nasa.gov/cgi-bin/mirador/presentNavigation.pl](http://mirador.gsfc.nasa.gov/cgi-bin/mirador/presentNavigation.pl?tree=project&project=TRMM&dataGroup=Gridded)  
703 [?tree=project&project=TRMM&dataGroup=Gridded](http://mirador.gsfc.nasa.gov/cgi-bin/mirador/presentNavigation.pl?tree=project&project=TRMM&dataGroup=Gridded). TRMM 3B40RT data are downloaded  
704 from <ftp://trmmopen.nascom.nasa.gov/pub/merged/combinedMicro/>. TRMM 3B41RT data  
705 are downloaded from <ftp://trmmopen.nascom.nasa.gov/pub/merged/calibratedIR/>.  
706 TRMM3B42RT data are downloaded from [ftp://trmmopen.nascom.nasa.gov/pub/merged/mer](ftp://trmmopen.nascom.nasa.gov/pub/merged/mergeIRMicr)  
707 [geIRMicr/](ftp://trmmopen.nascom.nasa.gov/pub/merged/mergeIRMicr). PERSIANN data are downloaded from [http://chrs.web.uci.edu/persiann/data.ht](http://chrs.web.uci.edu/persiann/data.html)  
708 [ml](http://chrs.web.uci.edu/persiann/data.html). GSMAP\_MVK data are downloaded from [http://sharaku.eorc.jaxa.jp/GSMaP\\_crest/](http://sharaku.eorc.jaxa.jp/GSMaP_crest/). The

709 GLDAS data are downloaded from <http://mirador.gsfc.nasa.gov/cgi-bin/mirador/homepageAl>  
710 [t.pl?keyword=GLDAS\\_NOAH025SUBP\\_3H](http://mirador.gsfc.nasa.gov/cgi-bin/mirador/homepageAl.t.pl?keyword=GLDAS_NOAH025SUBP_3H). The data of Biliu basin were obtained from the  
711 Biliu reservoir administration.

712

## 713 **References**

714

715 Aonashi, K., Awaka, J., Hirose, M., Kozu, T., Kubota, T., Liu, G., Shige, S., Kida, S., Seto, S.,  
716 Takahashi, N., and Takayabu, Y. N.: GSMaP Passive Microwave Precipitation Retrieval  
717 Algorithm: Algorithm Description and Validation, *Journal of the Meteorological Society*  
718 of Japan, 87A, 119-136, 10.2151/jmsj.87A.119, 2009.

719 Artan, G., Gadain, H., Smith, J. L., Asante, K., Bandaragoda, C. J., and Verdin, J. P.:  
720 Adequacy of satellite derived rainfall data for stream flow modeling, *Natural Hazards*, 43,  
721 167-185, 10.1007/s11069-007-9121-6, 2007.

722 Asadullah, A., McIntyre, N., and Kigobe, M. A. X.: Evaluation of five satellite products for  
723 estimation of rainfall over Uganda, *Hydrological Sciences Journal*, 53, 1137-1150,  
724 10.1623/hysj.53.6.1137, 2008.

725 Bastola, S., Ishidaira, H., and Takeuchi, K.: Regionalisation of hydrological model  
726 parameters under parameter uncertainty: A case study involving TOPMODEL and basins  
727 across the globe, *Journal of Hydrology*, 357, 188-206, 10.1016/j.jhydrol.2008.05.007,  
728 2008.

729 Betts, A. K., Chen, F., Mitchell, K. E., and Janjic, Z. I.: Assessment of the land surface and  
730 boundary layer models in two operational versions of the NCEP Eta Model using FIFE

731 data, Monthly Weather Review, 125, 2896-2916,  
732 10.1175/1520-0493(1997)125<2896:aotlsa>2.0.co;2, 1997.

733 Beven, K. J., and Binley, A.: The future of distributed models: model calibration and  
734 uncertainty prediction, Hydrological Processes, 6, 279-298, 10.1002/hyp.3360060305,  
735 1992.

736 Beven, K. J., and Freer, J. E.: A dynamic TOPMODEL, Hydrological Processes, 15,  
737 1993-2011, 10.1002/hyp.252, 2001a.

738 Beven, K. J., and Freer, J. E.: Equifinality, data assimilation, and uncertainty estimation in  
739 mechanistic modelling of complex environmental systems using the GLUE methodology,  
740 Journal of Hydrology, 249, 11–29, 10.1016/S0022-1694(01)00421-8, 2001b.

741 Beven, K. J., and Kirkby, M. J.: A physically based, variable contributing area model of basin  
742 hydrology, Hydrological Sciences Bulletin, 24, 43-69, 10.1080/02626667909491834,  
743 1979.

744 Blasone, R.-S., Vrugt, J. A., Madsen, H., Rosbjerg, D., Robinson, B. A., and Zyvoloski, G. A.:  
745 Generalized likelihood uncertainty estimation (GLUE) using adaptive Markov Chain  
746 Monte Carlo sampling, Advances in Water Resources, 31, 630-648,  
747 10.1016/j.advwatres.2007.12.003, 2008.

748 Blazkova, S., and Beven, K.: Flood frequency prediction for data limited catchments in the  
749 Czech Republic using a stochastic rainfall model and TOPMODEL, Journal of Hydrology,  
750 195, 256-278, 10.1016/S0022-1694(96)03238-6, 1997.

751 Bosshard, T., Carambia, M., Goergen, K., Kotlarski, S., Krahe, P., Zappa, M., and Schär, C.:

752 Quantifying uncertainty sources in an ensemble of hydrological climate-impact  
753 projections, *Water Resources Research*, 49, 1523-1536, 10.1029/2011wr011533, 2013.

754 Bouilloud, L., Chancibault, K., Vincendon, B., Ducrocq, V., Habets, F., Saulnier, G.-M.,  
755 Anquetin, S., Martin, E., and Noilhan, J.: Coupling the ISBA Land Surface Model and the  
756 TOPMODEL Hydrological Model for Mediterranean Flash-Flood Forecasting:  
757 Description, Calibration, and Validation, *Journal of Hydrometeorology*, 11, 315-333,  
758 10.1175/2009jhm1163.1, 2010.

759 Buarque, D. C., de Paiva, R. C. D., Clarke, R. T., and Mendes, C. A. B.: A comparison of  
760 Amazon rainfall characteristics derived from TRMM, CMORPH and the Brazilian  
761 national rain gauge network, *Journal of Geophysical Research*, 116,  
762 10.1029/2011jd016060, 2011.

763 Cameron, D. S., Beven, K. J., Tawn, J., Blazkova, S., and Naden, P.: Flood frequency  
764 estimation by continuous simulation for a gauged upland catchment (with uncertainty),  
765 *Journal of Hydrology*, 219, 169-187, 10.1016/S0022-1694(99)00057-8, 1999.

766 Chen, F., Mitchell, K., Schaake, J., Xue, Y., Pan, H.-L., Koren, V., Duan, Q. Y., Ek, M., and  
767 Betts, A.: Modeling of land surface evaporation by four schemes and comparison with  
768 FIFE observations, *Journal of Geophysical Research*, 101, 7251, 10.1029/95jd02165,  
769 1996.

770 Chen, S., Hong, Y., Cao, Q., Gourley, J. J., Kirstetter, P.-E., Yong, B., Tian, Y., Zhang, Z.,  
771 Shen, Y., Hu, J., and Hardy, J.: Similarity and difference of the two successive V6 and V7  
772 TRMM multisatellite precipitation analysis performance over China, *Journal of*



773 Geophysical Research: Atmospheres, 118, 13,060-013,074, 10.1002/2013jd019964,  
774 2013a.

775 Chen, S., Hong, Y., Gourley, J. J., Huffman, G. J., Tian, Y., Cao, Q., Yong, B., Kirstetter, P.-E.,  
776 Hu, J., Hardy, J., Li, Z., Khan, S. I., and Xue, X.: Evaluation of the successive V6 and V7  
777 TRMM multisatellite precipitation analysis over the Continental United States, Water  
778 Resources Research, 49, 8174-8186, 10.1002/2012wr012795, 2013b.

779 Dai, Y., Zeng, X., Dickinson, R. E., Baker, I., Bonan, G. B., Bosilovich, M. G., Denning, A.  
780 S., Dirmeyer, P. A., Houser, P. R., Niu, G., Oleson, K. W., Schlosser, C. A., and Yang,  
781 Z.-L.: The Common Land Model, Bulletin of the American Meteorological Society, 84,  
782 1013-1023, 10.1175/bams-84-8-1013, 2003.

783 Dinku, T., Connor, S. J., Ceccato, P., and Ropelewski, C. F.: Comparison of global gridded  
784 precipitation products over a mountainous region of Africa, International Journal of  
785 Climatology, 28, 1627-1638, 10.1002/joc.1669, 2008.

786 Ebert, E. E., Janowiak, J. E., and Kidd, C.: Comparison of Near-Real-Time Precipitation  
787 Estimates from Satellite Observations and Numerical Models, Bulletin of the American  
788 Meteorological Society, 88, 47-64, 10.1175/bams-88-1-47, 2007.

789 Ek, M. B.: Implementation of Noah land surface model advances in the National Centers for  
790 Environmental Prediction operational mesoscale Eta model, Journal of Geophysical  
791 Research, 108, 10.1029/2002jd003296, 2003.

792 Freer, J. E., Beven, K. J., and Ambrose, B.: Bayesian Estimation of Uncertainty in Runoff  
793 Prediction and the Value of Data: An Application of the GLUE Approach, Water

794 Resources Research, 32, 2161-2173, 10.1029/95wr03723, 1996.

795 Gallart, F., Latron, J., Llorens, P., and Beven, K. J.: Upscaling discrete internal observations  
796 for obtaining catchment-averaged TOPMODEL parameters in a small Mediterranean  
797 mountain basin, Physics and Chemistry of the Earth, 33, 1090-1094,  
798 10.1016/j.pce.2008.03.003, 2008.

799 Gao, Y. C., and Liu, M. F.: Evaluation of high-resolution satellite precipitation products using  
800 rain gauge observations over the Tibetan Plateau, Hydrology and Earth System Sciences,  
801 17, 837-849, 10.5194/hess-17-837-2013, 2013.

802 Heidari, A., Saghafian, B., and Maknoon, R.: Assessment of flood forecasting lead time based  
803 on generalized likelihood uncertainty estimation approach, Stochastic Environmental  
804 Research and Risk Assessment, 20, 363-380, 10.1007/s00477-006-0032-y, 2006.

805 Herman, J. D., Reed, P. M., and Wagener, T.: Time - varying sensitivity analysis clarifies the  
806 effects of watershed model formulation on model behavior, Water Resources Research,  
807 49, 1400-1414, 10.1002/wrcr.20124, 2013.

808 Hong, Y., Hsu, K.-l., Moradkhani, H., and Sorooshian, S.: Uncertainty quantification of  
809 satellite precipitation estimation and Monte Carlo assessment of the error propagation  
810 into hydrologic response, Water Resources Research, 42, 10.1029/2005wr004398, 2006.

811 Hossain, F., and Anagnostou, E. N.: Assessment of a stochastic interpolation based parameter  
812 sampling scheme for efficient uncertainty analyses of hydrologic models, Computers &  
813 Geosciences, 31, 497-512, 10.1016/j.cageo.2004.11.001, 2005.

814 Huffman, G. J., Bolvin, D. T., Nelkin, E. J., Wolff, D. B., Adler, R. F., Gu, G., Hong, Y.,

815 Bowman, K. P., and Stocker, E. F.: The TRMM Multisatellite Precipitation Analysis  
816 (TMPA): Quasi-Global, Multiyear, Combined-Sensor Precipitation Estimates at Fine  
817 Scales, *Journal of Hydrometeorology*, 8, 38-55, 10.1175/jhm560.1, 2007.

818 Jiang, S., Ren, L., Hong, Y., Yong, B., Yang, X., Yuan, F., and Ma, M.: Comprehensive  
819 evaluation of multi-satellite precipitation products with a dense rain gauge network and  
820 optimally merging their simulated hydrological flows using the Bayesian model  
821 averaging method, *Journal of Hydrology*, 452-453, 213-225,  
822 10.1016/j.jhydrol.2012.05.055, 2012.

823 Kato, H., Rodell, M., Beyrich, F., Cleugh, H., Gorsel, E. v., Liu, H., and Meyers, T. P.:  
824 Sensitivity of Land Surface Simulations to Model Physics, Land Characteristics, and  
825 Forcings, at Four CEOP Sites, *Journal of the Meteorological Society of Japan*, 85A,  
826 187-204, 10.2151/jmsj.85A.187, 2007.

827 Kneis, D., Chatterjee, C., and Singh, R.: Evaluation of TRMM rainfall estimates over a large  
828 Indian river basin (Mahanadi), *Hydrology and Earth System Sciences*, 18, 2493-2502,  
829 10.5194/hess-18-2493-2014, 2014.

830 Koren, V., Schaake, J., Mitchell, K., Duan, Q. Y., Chen, F., and Baker, J. M.: A  
831 parameterization of snowpack and frozen ground intended for NCEP weather and climate  
832 models, *Journal of Geophysical Research*, 104, 19569, 10.1029/1999jd900232, 1999.

833 Koster, R. D., and Suarez, M. J.: Modeling the land surface boundary in climate models as a  
834 composite of independent vegetation stands, *Journal of Geophysical  
835 Research-Atmospheres*, 97, 2697-2715, 10.1029/91JD01696, 1992.

836 Kubota, T., Shige, S., Hashizume, H., Aonashi, K., Takahashi, N., Seto, S., Hirose, M.,  
837 Takayabu, Y. N., Ushio, T., Nakagawa, K., Wanami, K., Kachi, M., and Okamoto, K.:  
838 Global precipitation map using satellite-borne microwave radiometers by the GSMaP  
839 project: Production and validation, *IEEE Transactions on Geoscience and Remote*  
840 *Sensing*, 45, 2259-2275, 10.1109/tgrs.2007.895337, 2007.

841 Kuczera, G., Kavetski, D., Franks, S., and Thyer, M.: Towards a Bayesian total error analysis  
842 of conceptual rainfall-runoff models: Characterising model error using storm-dependent  
843 parameters, *Journal of Hydrology*, 331, 161-177, 10.1016/j.jhydrol.2006.05.010, 2006.

844 Kuczera, G., and Parent, E.: Monte Carlo assessment of parameter uncertainty in conceptual  
845 catchment models- the Metropolis algorithm, *Journal of Hydrology*, 211, 69-85,  
846 10.1016/S0022-1694(98)00198-X, 1998.

847 Kummerow, C., Simpson, J., and Thiele, O.: The status of the Tropical Rainfall Measuring  
848 Mission (TRMM) after two years in orbit, *Journal of Applied Meteorology and*  
849 *Climatology* 39, 10.1175/1520-0450(2001)040<1965:TSOTTR>2.0.CO;2, 2000.

850 Li, Z., Yang, D., and Hong, Y.: Multi-scale evaluation of high-resolution multi-sensor blended  
851 global precipitation products over the Yangtze River, *Journal of Hydrology*, 500, 157-169,  
852 10.1016/j.jhydrol.2013.07.023, 2013.

853 Liang, X., Lettenmaier, D. P., Wood, E. F., and Burges, S. J.: A simple hydrologically based  
854 model of land-surface water and energy fluxes for general-circulation models, *Journal of*  
855 *Geophysical Research-Atmospheres*, 99, 14415-14428, 10.1029/94jd00483, 1994.

856 Müller, M. F., and Thompson, S. E.: Bias adjustment of satellite rainfall data through

857 stochastic modeling: Methods development and application to Nepal, *Advances in Water*  
858 *Resources*, 60, 121-134, 10.1016/j.advwatres.2013.08.004, 2013.

859 Maggioni, V., Vergara, H. J., Anagnostou, E. N., Gourley, J. J., Hong, Y., and Stampoulis, D.:  
860 Investigating the Applicability of Error Correction Ensembles of Satellite Rainfall  
861 Products in River Flow Simulations, *Journal of Hydrometeorology*, 14, 1194-1211,  
862 10.1175/jhm-d-12-074.1, 2013.

863 Meng, J., Li, L., Hao, Z., Wang, J., and Shao, Q.: Suitability of TRMM satellite rainfall in  
864 driving a distributed hydrological model in the source region of Yellow River, *Journal of*  
865 *Hydrology*, 509, 320-332, 10.1016/j.jhydrol.2013.11.049, 2014.

866 Nikolopoulos, E. I., Anagnostou, E. N., Hossain, F., Gebremichael, M., and Borga, M.:  
867 Understanding the Scale Relationships of Uncertainty Propagation of Satellite Rainfall  
868 through a Distributed Hydrologic Model, *Journal of Hydrometeorology*, 11, 520-532,  
869 10.1175/2009jhm1169.1, 2010.

870 Ochoa, A., Pineda, L., Crespo, P., and Willems, P.: Evaluation of TRMM 3B42 precipitation  
871 estimates and WRF retrospective precipitation simulation over the Pacific–Andean region  
872 of Ecuador and Peru, *Hydrology and Earth System Sciences*, 18, 3179-3193,  
873 10.5194/hess-18-3179-2014, 2014.

874 Pan, M., Li, H., and Wood, E.: Assessing the skill of satellite-based precipitation estimates in  
875 hydrologic applications, *Water Resources Research*, 46, 10.1029/2009wr008290, 2010.

876 Parton, W. J., and Logan, J. A.: A model for diurnal variation in soil and air temperature,  
877 *Agricultural Meteorology*, 23, 205-216, 10.1016/0002-1571(81)90105-9, 1981.

878 Peng, Z., Wang, Q. J., Bennett, J. C., Pokhrel, P., and Wang, Z.: Seasonal precipitation  
879 forecasts over China using monthly large-scale oceanic-atmospheric indices, *Journal of*  
880 *Hydrology*, 519, 792-802, 10.1016/j.jhydrol.2014.08.012, 2014a.

881 Peng, Z., Wang, Q. J., Bennett, J. C., Schepen, A., Pappenberger, F., Pokhrel, P., and Wang, Z.:  
882 Statistical calibration and bridging of ECMWF System4 outputs for forecasting seasonal  
883 precipitation over China, *Journal of Geophysical Research: Atmospheres*, 119, 7116-7135,  
884 10.1002/2013jd021162, 2014b.

885 Peters, N. E., Freer, J., and Beven, K.: Modelling hydrologic responses in a small forested  
886 catchment (Panola Mountain, Georgia, USA): a comparison of the original and a new  
887 dynamic TOPMODEL, *Hydrological Processes*, 17, 345-362, 10.1002/hyp.1128, 2003.

888 Qi, W., Zhang, C., Chu, J., and Zhou, H.: Sobol's sensitivity analysis for TOPMODEL  
889 hydrological model: A case study for the Biliu River Basin, China, *Journal of Hydrology*  
890 *and Environment Research*, 1, 1-10, 2013.

891 Qi, W., Zhang, C., Fu, G., and Zhou, H.: Global Land Data Assimilation System data  
892 assessment using a distributed biosphere hydrological model, *Journal of Hydrology*, 528,  
893 652-667, 10.1016/j.jhydrol.2015.07.011, 2015.

894 Qi, W., Zhang, C., Fu, G., and Zhou, H.: Quantifying dynamic sensitivity of optimization  
895 algorithm parameters to improve hydrological model calibration, *Journal of Hydrology*,  
896 533, 213-223, 10.1016/j.jhydrol.2015.11.052, 2016.

897 Rodell, M., Houser, P. R., Jambor, U., Gottschalck, J., Mitchell, K., Meng, C. J., Arsenault,  
898 K., Cosgrove, B., Radakovich, J., Bosilovich, M., Entin\*, J. K., Walker, J. P., Lohmann,

899 D., and Toll, D.: The Global Land Data Assimilation System, *Bulletin of the American*  
900 *Meteorological Society*, 85, 381-394, 10.1175/bams-85-3-381, 2004.

901 Sapriza-Azuri, G., Jódar, J., Navarro, V., Slooten, L. J., Carrera, J., and Gupta, H. V.: Impacts  
902 of rainfall spatial variability on hydrogeological response, *Water Resources Research*, 51,  
903 1300-1314, 10.1002/2014wr016168, 2015.

904 Sellers, P. J.: Modeling the Exchanges of Energy, Water, and Carbon Between Continents and  
905 the Atmosphere, *Science*, 275, 502-509, 10.1126/science.275.5299.502, 1997.

906 Sellers, P. J., Mintz, Y., Sud, Y. C., and Dalcher, A.: A Simple Biosphere Model (SIB) for Use  
907 within General Circulation Models, *Journal of the Atmospheric Sciences*, 43, 505-531,  
908 10.1175/1520-0469(1986)043<0505:ASBMFU>2.0.CO;2, 1986.

909 Sellers, P. J., Randall, D. A., Collatz, G. J., Berry, J. A., Field, C. B., Dazlich, D. A., Zhang,  
910 C., Collelo, G. D., and Bounoua, L.: A Revised Land Surface Parameterization (SiB2) for  
911 Atmospheric GCMS. Part I: Model Formulation, *Journal of Climate*, 9, 676-705,  
912 10.1175/1520-0442(1996)009<0676:ARLSPF>2.0.CO;2, 1996.

913 Serpetzoglou, E., Anagnostou, E. N., Papadopoulos, A., Nikolopoulos, E. I., and Maggioni, V.:  
914 Error Propagation of Remote Sensing Rainfall Estimates in Soil Moisture Prediction from  
915 a Land Surface Model, *Journal of Hydrometeorology*, 11, 705-720,  
916 10.1175/2009jhm1166.1, 2010.

917 Shou, Y., and Xu, J.: The rainstorm and mesoscale convective systems over northeast China  
918 in june 2005 I: A synthetic analysis of mcs by conventional observations and satellite data  
919 (in Chinese), *Acta Meteorologica Sinica*, 65, 160-170, 2007a.

920 Shou, Y., and Xu, J.: The rainstorm and mesoscale convective systems over northeast China  
921 in June 2005 II: A synthetic analysis of MCS's dynamical structure by radar and satellite  
922 observations (in Chinese), *Acta Meteorologica Sinica*, 65, 171-182, 2007b.

923 Shrestha, M., Wang, L., Koike, T., Tsutsui, H., Xue, Y., and Hirabayashi, Y.: Correcting  
924 basin-scale snowfall in a mountainous basin using a distributed snowmelt model and  
925 remote sensing data, *Hydrol. Earth Syst. Sci. Discuss.*, 10, 11711-11753,  
926 10.5194/hessd-10-11711-2013, 2013.

927 Sorooshian, S., Gao, X., Hsu, K., Maddox, R. A., Hong, Y., Gupta, H. V., and Imam, B.:  
928 Diurnal Variability of Tropical Rainfall Retrieved from Combined GOES and TRMM  
929 Satellite Information, *Journal of Climate*, 15, 983-1001,  
930 10.1175/1520-0442(2002)015<0983:DVOTRR>2.0.CO;2, 2002.

931 Sorooshian, S., Hsu, K. L., Gao, X., Gupta, H. V., Imam, B., and Braithwaite, D.: Evaluation  
932 of PERSIANN system satellite-based estimates of tropical rainfall, *Bulletin of the*  
933 *American Meteorological Society*, 81, 2035-2046,  
934 10.1175/1520-0477(2000)081<2035:eopsse>2.3.co;2, 2000.

935 Sorooshian, S., Lawford, R. G., Try, P., Rossow, W., Roads, J., Polcher, J., Sommeria, G., and  
936 Schifer, R.: Water and energy cycles: Investigating the links, *WMO Bull.*, 54, 2005.

937 Su, F., Hong, Y., and Lettenmaier, D. P.: Evaluation of TRMM Multisatellite Precipitation  
938 Analysis (TMPA) and Its Utility in Hydrologic Prediction in the La Plata Basin, *Journal*  
939 *of Hydrometeorology*, 9, 622-640, 10.1175/2007jhm944.1, 2008.

940 Tapiador, F. J., Turk, F. J., Petersen, W., Hou, A. Y., García-Ortega, E., Machado, L. A. T.,



941 Angelis, C. F., Salio, P., Kidd, C., Huffman, G. J., and de Castro, M.: Global precipitation  
942 measurement: Methods, datasets and applications, *Atmospheric Research*, 104-105, 70-97,  
943 10.1016/j.atmosres.2011.10.021, 2012.

944 Tolson, B. A., and Shoemaker, C. A.: Dynamically dimensioned search algorithm for  
945 computationally efficient watershed model calibration, *Water Resources Research*, 43,  
946 10.1029/2005wr004723, 2007.

947 Vrugt, J. A., ter Braak, C. J. F., Gupta, H. V., and Robinson, B. A.: Equifinality of formal  
948 (DREAM) and informal (GLUE) Bayesian approaches in hydrologic modeling?,  
949 *Stochastic Environmental Research and Risk Assessment*, 23, 1011-1026,  
950 10.1007/s00477-008-0274-y, 2009b.

951 Wang, D., Wang, G., and Anagnostou, E. N.: Use of Satellite-Based Precipitation Observation  
952 in Improving the Parameterization of Canopy Hydrological Processes in Land Surface  
953 Models, *Journal of Hydrometeorology*, 6, 745-763, 10.1175/JHM438.1, 2005.

954 Wang, F., Wang, L., Koike, T., Zhou, H., Yang, K., Wang, A., and Li, W.: Evaluation and  
955 application of a fine-resolution global data set in a semiarid mesoscale river basin with a  
956 distributed biosphere hydrological model, *Journal of Geophysical Research*, 116,  
957 10.1029/2011jd015990, 2011.

958 Wang, F., Wang, L., Zhou, H., Saavedra Valeriano, O. C., Koike, T., and Li, W.: Ensemble  
959 hydrological prediction-based real-time optimization of a multiobjective reservoir during  
960 flood season in a semiarid basin with global numerical weather predictions, *Water  
961 Resources Research*, 48, 10.1029/2011wr011366, 2012.

962 Wang, L., Koike, T., Yang, D. W., and Yang, K.: Improving the hydrology of the Simple  
963 Biosphere Model 2 and its evaluation within the framework of a distributed hydrological  
964 model, *Hydrological Sciences Journal-Journal Des Sciences Hydrologiques*, 54,  
965 989-1006, 10.1623/hysj.54.6.989, 2009a.

966 Wang, L., Koike, T., Yang, K., Jackson, T. J., Bindlish, R., and Yang, D.: Development of a  
967 distributed biosphere hydrological model and its evaluation with the Southern Great  
968 Plains Experiments (SGP97 and SGP99), *Journal of Geophysical Research*, 114,  
969 10.1029/2008jd010800, 2009b.

970 Wang, L., Koike, T., Yang, K., Jin, R., and Li, H.: Frozen soil parameterization in a  
971 distributed biosphere hydrological model, *Hydrol. Earth Syst. Sci.*, 14, 557-571,  
972 10.5194/hess-14-557-2010, 2010a.

973 Wang, L., Koike, T., Yang, K., and Yeh, P. J.-F.: Assessment of a distributed biosphere  
974 hydrological model against streamflow and MODIS land surface temperature in the upper  
975 Tone River Basin, *Journal of Hydrology*, 377, 21-34, 10.1016/j.jhydrol.2009.08.005,  
976 2009c.

977 Wang, L., Wang, Z., Koike, T., Yin, H., Yang, D., and He, S.: The assessment of surface water  
978 resources for the semi-arid Yongding River Basin from 1956 to 2000 and the impact of  
979 land use change, *Hydrological Processes*, 24, 1123-1132, 10.1002/hyp.7566, 2010b.

980 Xie, P., Chen, M., Yang, S., Yatagai, A., Hayasaka, T., Fukushima, Y., and Liu, C.: A  
981 Gauge-Based Analysis of Daily Precipitation over East Asia, *Journal of*  
982 *Hydrometeorology*, 8, 607-626, 10.1175/jhm583.1, 2007.

983 Xue, X., Hong, Y., Limaye, A. S., Gourley, J. J., Huffman, G. J., Khan, S. I., Dorji, C., and  
984 Chen, S.: Statistical and hydrological evaluation of TRMM-based Multi-satellite  
985 Precipitation Analysis over the Wangchu Basin of Bhutan: Are the latest satellite  
986 precipitation products 3B42V7 ready for use in ungauged basins?, *Journal of Hydrology*,  
987 499, 91-99, 10.1016/j.jhydrol.2013.06.042, 2013.

988 Yang, D.: Distributed hydrological model using hillslope discretization based on catchment  
989 area function: development and applications, PHD, University of Tokyo, Tokyo, 1998.

990 Yang, K., Koike, T., and Ye, B.: Improving estimation of hourly, daily, and monthly solar  
991 radiation by importing global data sets, *Agricultural and Forest Meteorology*, 137, 43-55,  
992 10.1016/j.agrformet.2006.02.001, 2006.

993 Yatagai, A., Kamiguchi, K., Arakawa, O., Hamada, A., Yasutomi, N., and Kitoh, A.:  
994 APHRODITE: Constructing a Long-Term Daily Gridded Precipitation Dataset for Asia  
995 Based on a Dense Network of Rain Gauges, *Bulletin of the American Meteorological*  
996 *Society*, 93, 1401-1415, 10.1175/bams-d-11-00122.1, 2012.

997 Yong, B., Chen, B., Gourley, J. J., Ren, L., Hong, Y., Chen, X., Wang, W., Chen, S., and Gong,  
998 L.: Intercomparison of the Version-6 and Version-7 TMPA precipitation products over  
999 high and low latitudes basins with independent gauge networks: Is the newer version  
1000 better in both real-time and post-real-time analysis for water resources and hydrologic  
1001 extremes?, *Journal of Hydrology*, 508, 77-87, 10.1016/j.jhydrol.2013.10.050, 2014.

1002 Yong, B., Hong, Y., Ren, L.-L., Gourley, J. J., Huffman, G. J., Chen, X., Wang, W., and Khan,  
1003 S. I.: Assessment of evolving TRMM-based multisatellite real-time precipitation

1004 estimation methods and their impacts on hydrologic prediction in a high latitude basin,  
1005 Journal of Geophysical Research, 117, 10.1029/2011jd017069, 2012.

1006 Yong, B., Ren, L.-L., Hong, Y., Wang, J.-H., Gourley, J. J., Jiang, S.-H., Chen, X., and Wang,  
1007 W.: Hydrologic evaluation of Multisatellite Precipitation Analysis standard precipitation  
1008 products in basins beyond its inclined latitude band: A case study in Laohahe basin, China,  
1009 Water Resources Research, 46, 10.1029/2009wr008965, 2010.

1010 Yuan, M., Li, Z., and Zhang, X.: Analysis of a meso scale convective system during a brief  
1011 torrential rain event in Northeast China (in Chinese), Acta Meteorologica Sinica, 68,  
1012 125-136, 10.11676/qxxb2010.013, 2010.

1013 Zhao, T., and Yatagai, A.: Evaluation of TRMM 3B42 product using a new gauge-based  
1014 analysis of daily precipitation over China, International Journal of Climatology, 34,  
1015 2749-2762, 10.1002/joc.3872, 2014.

1016 Zhou, T., Yu, R., Chen, H., Dai, A., and Pan, Y.: Summer Precipitation Frequency, Intensity,  
1017 and Diurnal Cycle over China: A Comparison of Satellite Data with Rain Gauge  
1018 Observations, Journal of Climate, 21, 3997-4010, 10.1175/2008jcli2028.1, 2008.

1019 Zhou, X. Y., Zhang, Y. Q., Yang, Y. H., Yang, Y. M., and Han, S. M.: Evaluation of anomalies  
1020 in GLDAS-1996 dataset, Water Science and Technology, 67, 1718-1727,  
1021 10.2166/wst.2013.043, 2013.

1022

1023 Table 1 Precipitation products

Product	Spatial resolution	Temporal resolution	Areal coverage	Start date	Type
TRMM3B42	0.25°	3h	Global 50°N-S	1 Jan 1998	PR+IR+MW+gauge+HM
TRMM3B42RT	0.25°	3h	Global 50°N-S	1 Mar 2000	IR+MW
GLDAS/Noah	0.25°	3h	Global 90°N-60°S	24 Feb 2000	IR+MW+gauge
GSMAP-MVK+	0.1°	1h	Global 60°N-S	1 Mar 2000	IR+MW+CMV
PRRSIANN	0.25°	3h	Global 60°N-S	1 Mar 2000	PR+IR+MW+ANN
APHRODITE	0.25°	1day	60°E-150°E, 15°S-55°N	1 Jan 1961 to 2007	gauge

1024 PR: precipitation radar; IR: infrared estimation; MW: microwave estimation; HM: histogram

1025 matching; CMV: cloud motion vectors; ANN: artificial neural network.

1026

1027 Table 2 WEB-DHM parameters

Symbol (unit)	Brief description	Basin-averaged value
<i>KS</i> (mm/h)	Saturated hydraulic conductivity for soil surface	26.43
<i>Anik</i>	Hydraulic conductivity anisotropy ratio	11.49
<i>Sstmax</i> (mm)	Maximum surface water storage	42.75
<i>Kg</i> (mm/h)	Hydraulic conductivity for groundwater	0.36
<i>alpha</i>	van Genuchten parameter	0.01
<i>n</i>	van Genuchten parameter	1.88

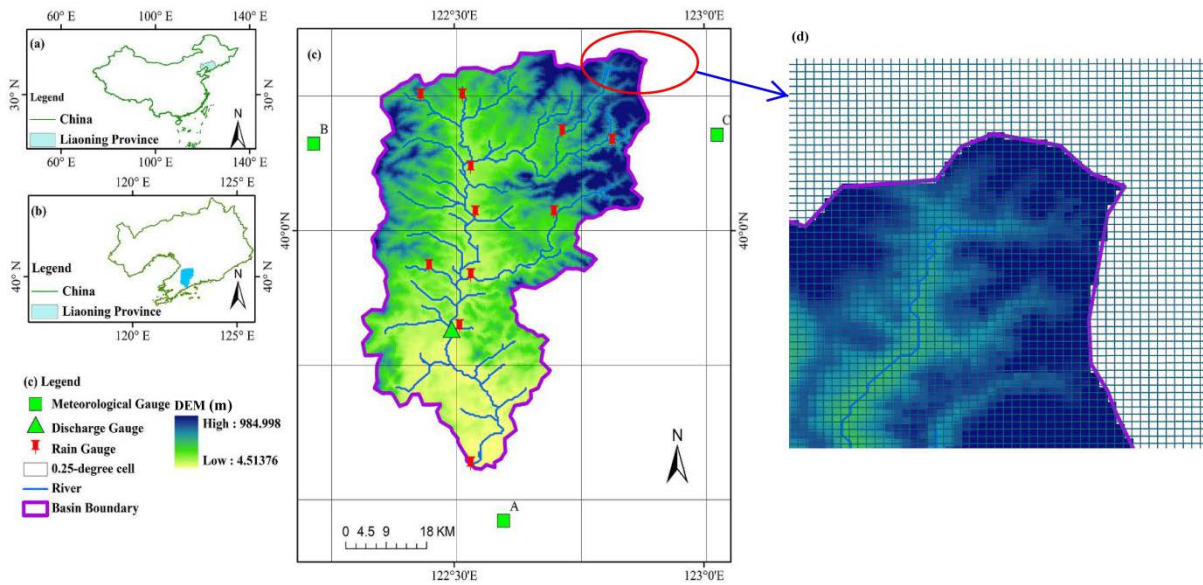
1028

1029 Table 3 TOPMODEL parameters

Name (unit)	Description	Lower bound	Upper bound	Calibration
$SZM$ (m)	form of the exponential decline in conductivity	0.01	0.04	0.019
$LNT0$ ( $m^2 h^{-1}$ )	log value of effective lateral saturated transmissivity	-25	1	-11.911
$RV$ ( $m h^{-1}$ )	hill slope routing velocity	2000	5000	2608.4
$SR_{max}$ (m)	maximum root zone storage	0.001	0.01	0.006
$SR_0$ (m)	initial root zone deficit	0	0.01	0.005
$TD$ ( $m h^{-1}$ )	unsaturated zone time delay per unit deficit	2	4	2.885

1030

1031

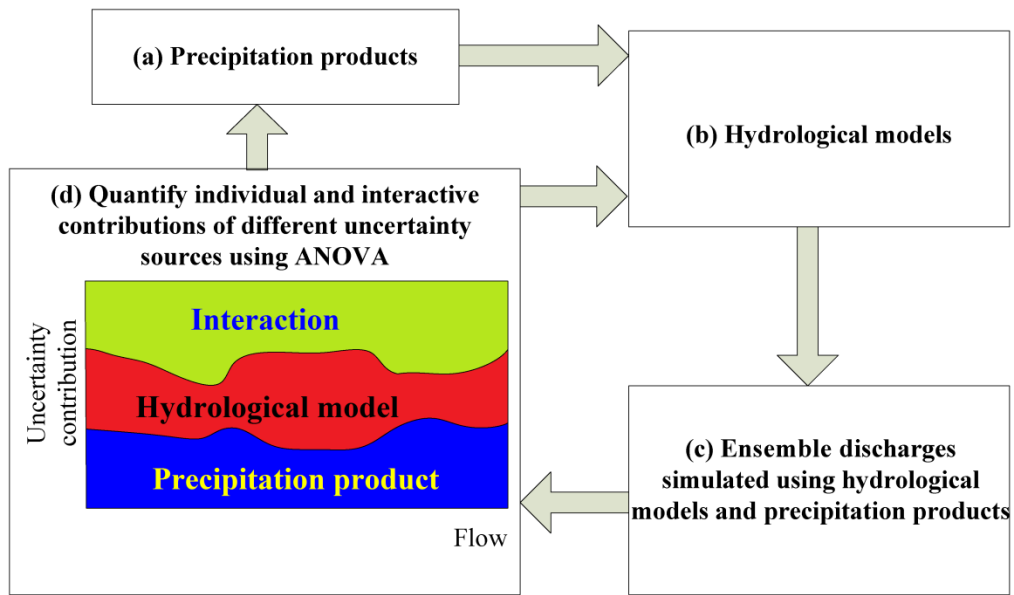


1032

1033 Fig. 1 Biliu basin: (a) the location of Liaoning province within China; (b) the location of  
 1034 Biliu basin within Liaoning province; (c) the distributions of rain gauges, discharge gauge,  
 1035 automatic weather stations, digital elevation model, and diagrammatic 0.25-degree  
 1036 precipitation cells; and (d) diagrammatic description of downscaling the 0.25-degree  
 1037 precipitation cells to 300 m × 300 m cells, and retrieving the 300 m × 300 m cells located  
 1038 within the basin boundary.

1039

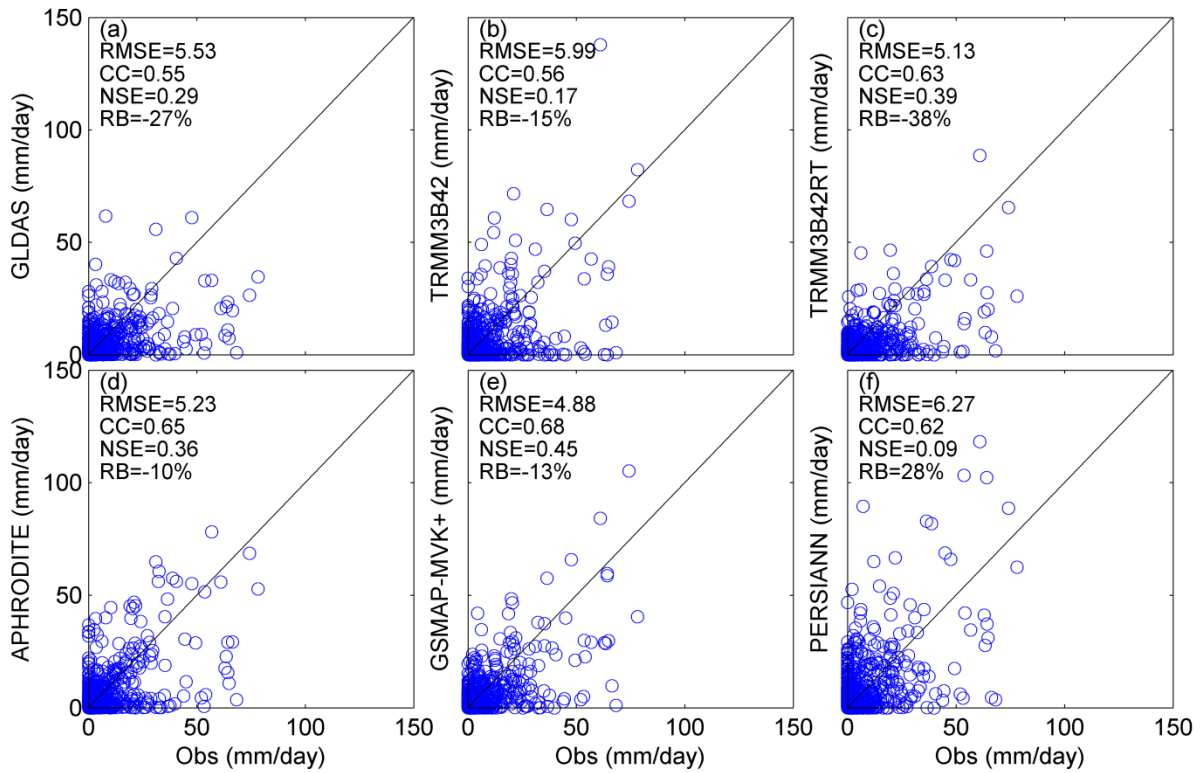




1040

1041 Fig. 2 Diagrammatic flowchart of the proposed framework for quantification of uncertainty  
 1042 contributions to ensemble discharges simulated using precipitation products on the basis of  
 1043 the analysis of variance (ANOVA) approach.

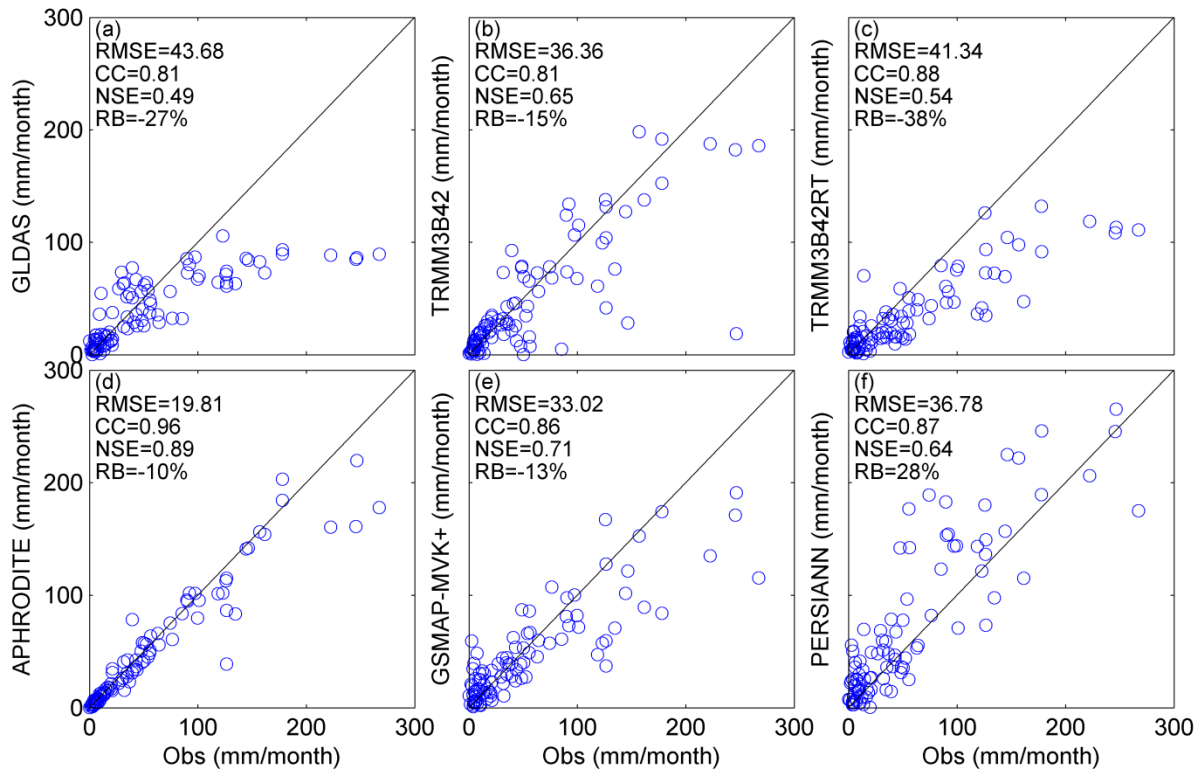
1044



1045

1046 Fig. 3 Scatterplots of basin-averaged precipitation products versus gauge observations at a  
 1047 daily scale.

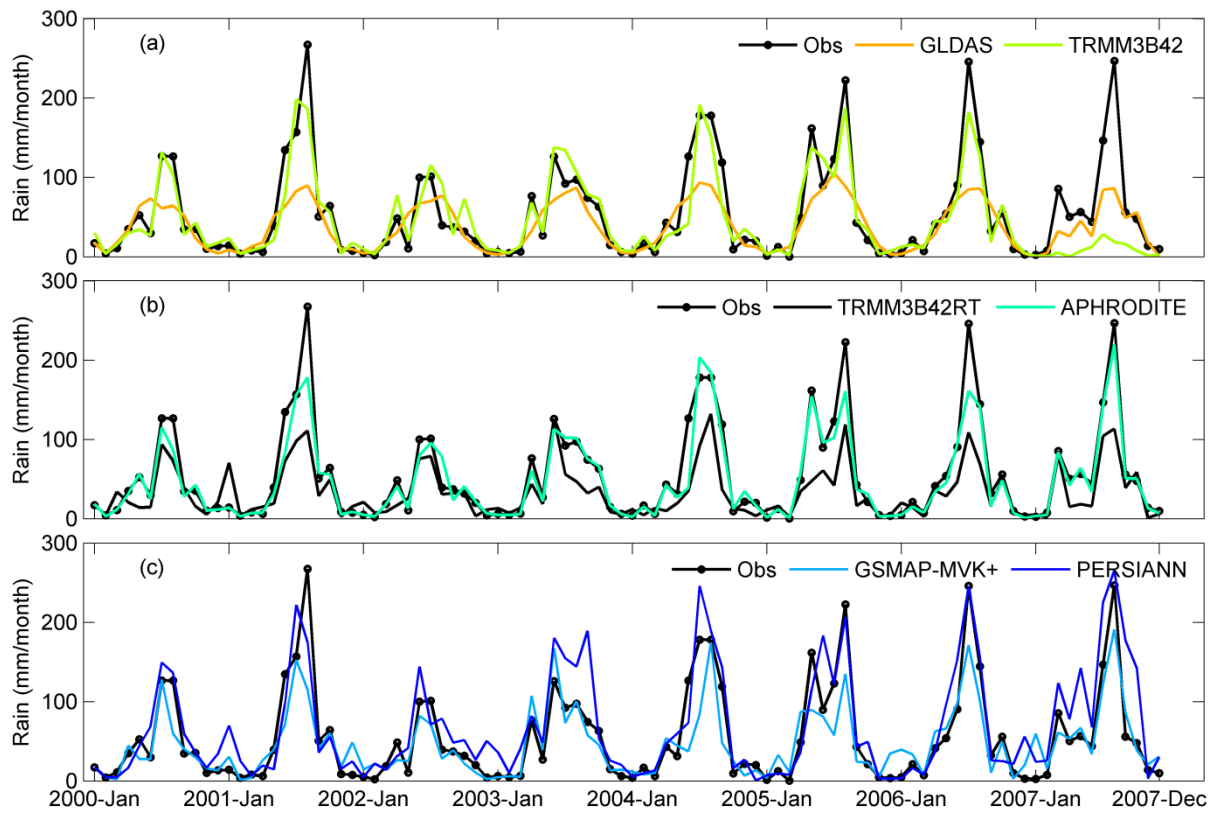
1048



1049

1050 Fig. 4 Scatterplots of basin-averaged precipitation products versus gauge observations at a  
 1051 monthly scale.

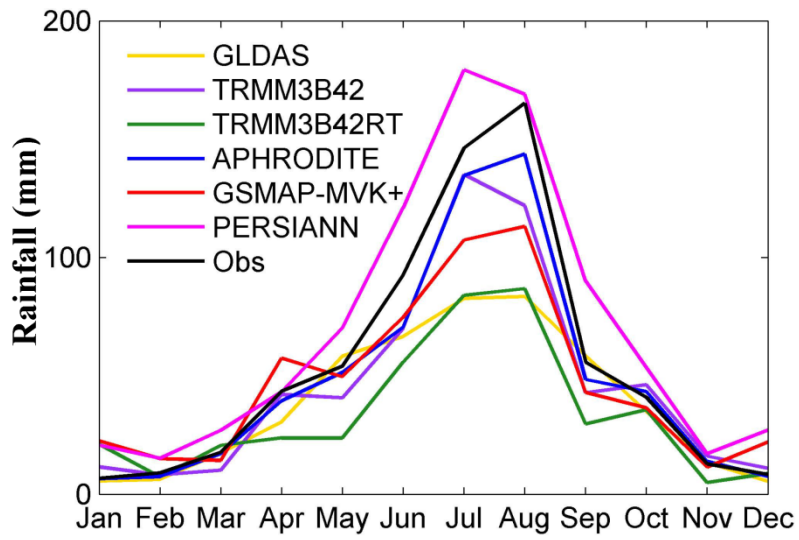
1052



1053

1054 Fig. 5 Time series plots of basin-averaged precipitation product values versus gauge  
 1055 observations at monthly scale.

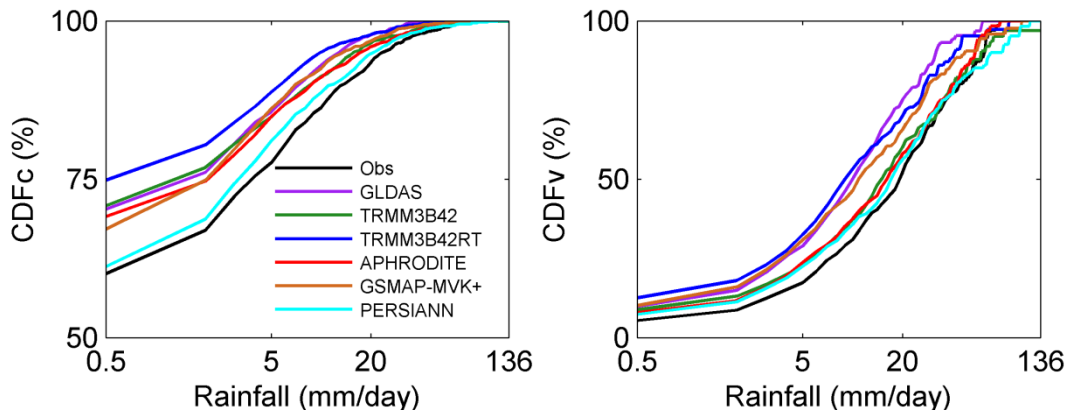
1056



1057

1058 Fig. 6 Inter-annual basin-averaged monthly precipitation.

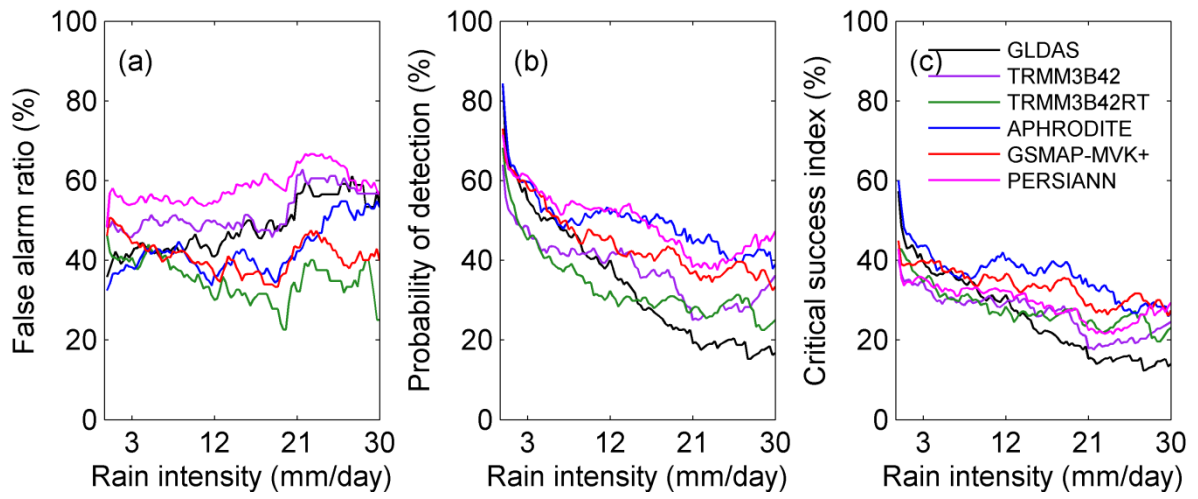
1059



1060

1061 Fig. 7 Probability distributions of the six precipitation products by occurrence (CDFc) and  
 1062 volume (CDFv).

1063

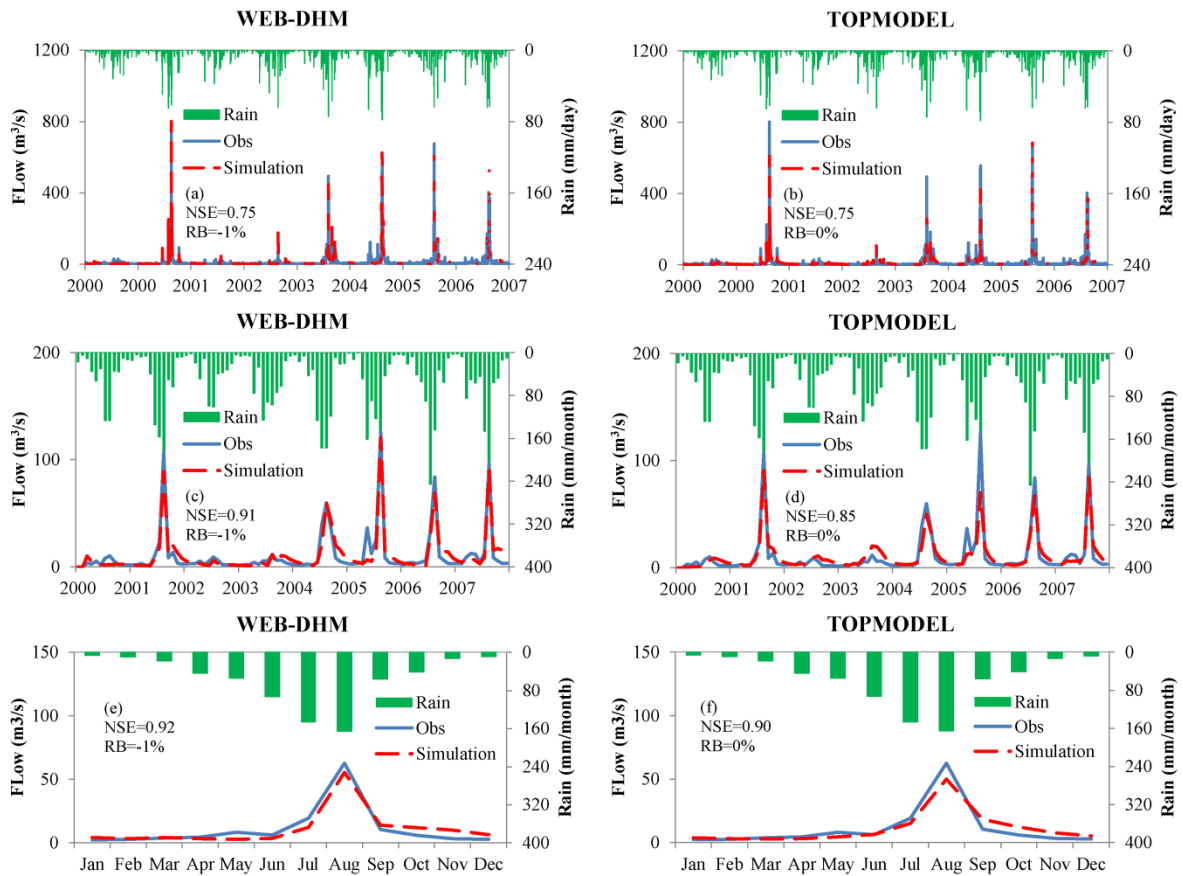


1064

1065 Fig. 8 False alarm ratio, probability of detection and critical success index for the six

1066 precipitation products.

1067



1068

1069 Fig. 9 Observed and simulated flows using WEB-DHM and TOPMODEL from 2000 to 2007:

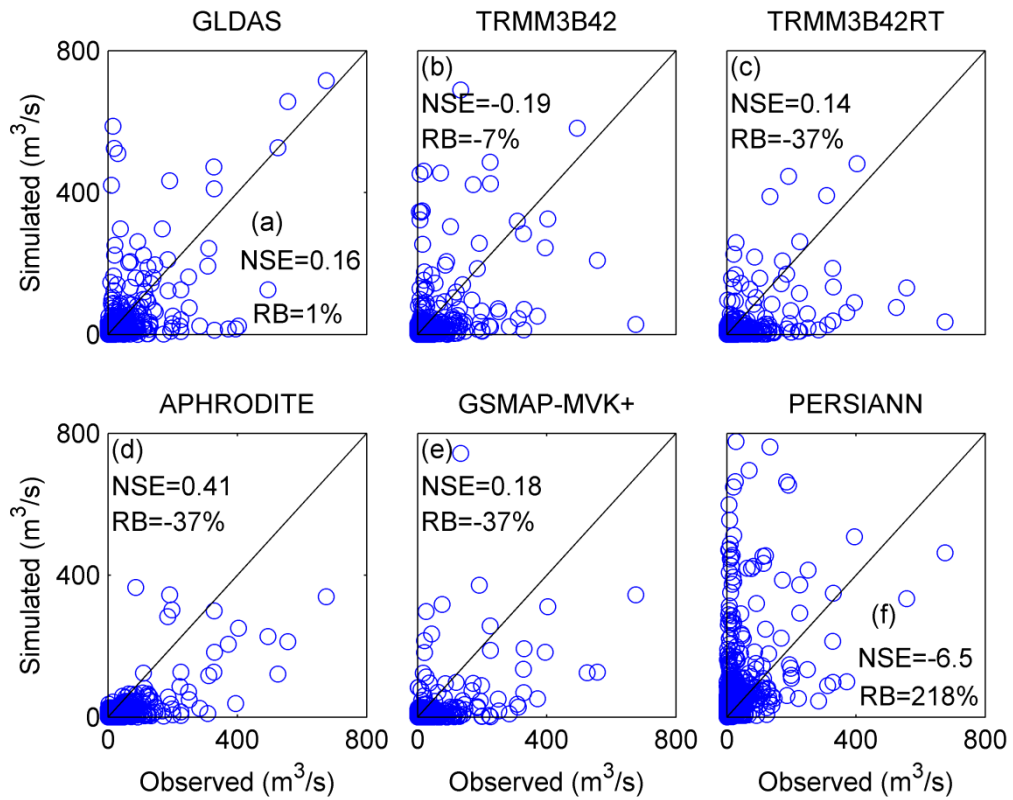
1070 (a), (c) and (e) are daily, monthly and inter-annual simulations using WEB-DHM respectively;

1071 (b), (d) and (f) are daily, monthly and inter-annual simulations using TOPMODEL

1072 respectively.

1073

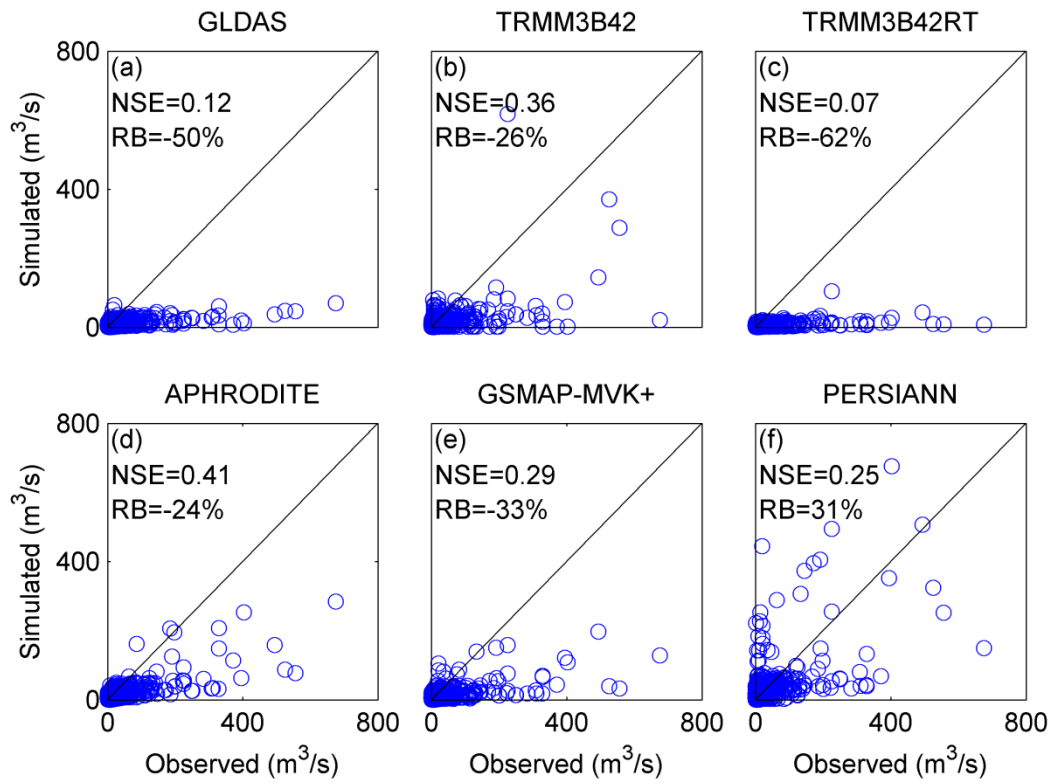




1074

1075 Fig. 10 Scatterplots of simulated discharges with WEB-DHM against gauge observations at a  
 1076 daily scale.

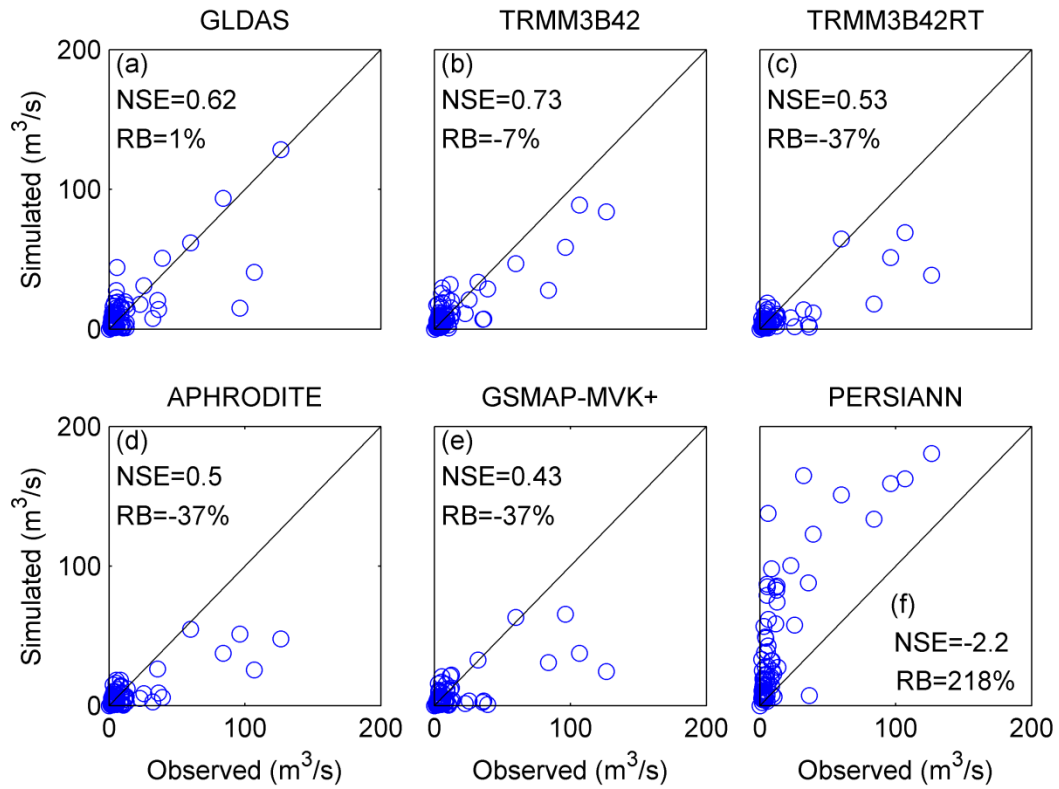
1077



1078

1079 Fig. 11 Scatterplots of simulated discharges with TOPMODEL against gauge observations at  
 1080 a daily scale.

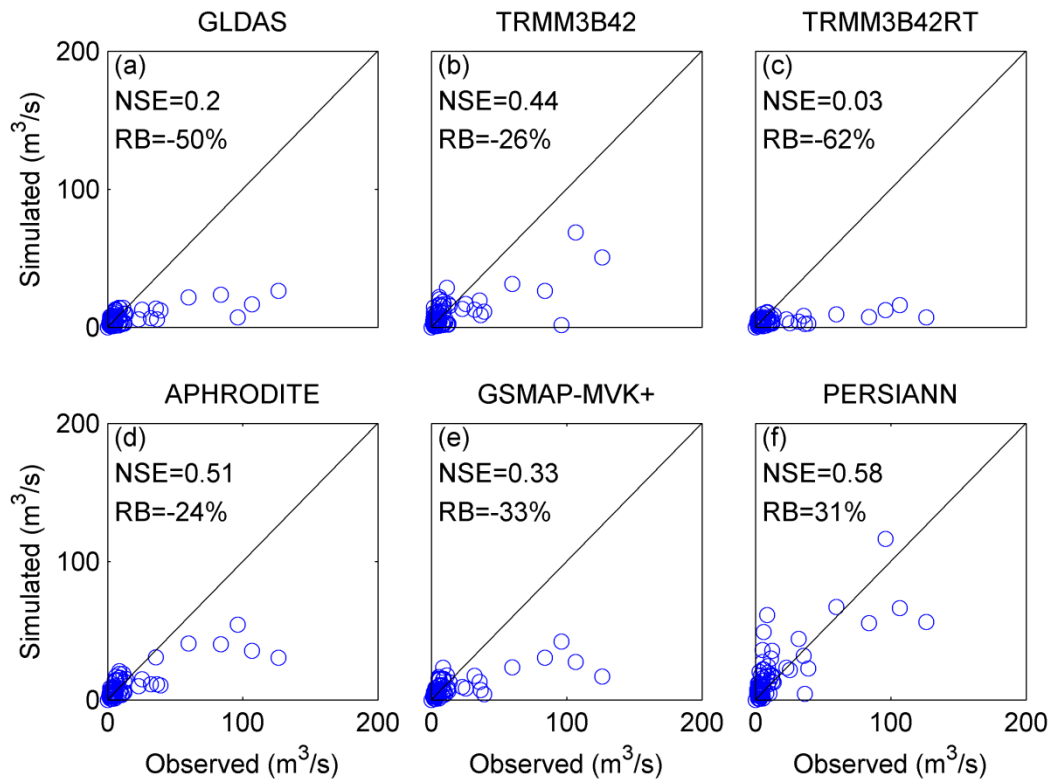
1081



1082

1083 Fig. 12 Scatterplots of simulated flows with WEB-DHM against gauge observations at a  
 1084 monthly scale.

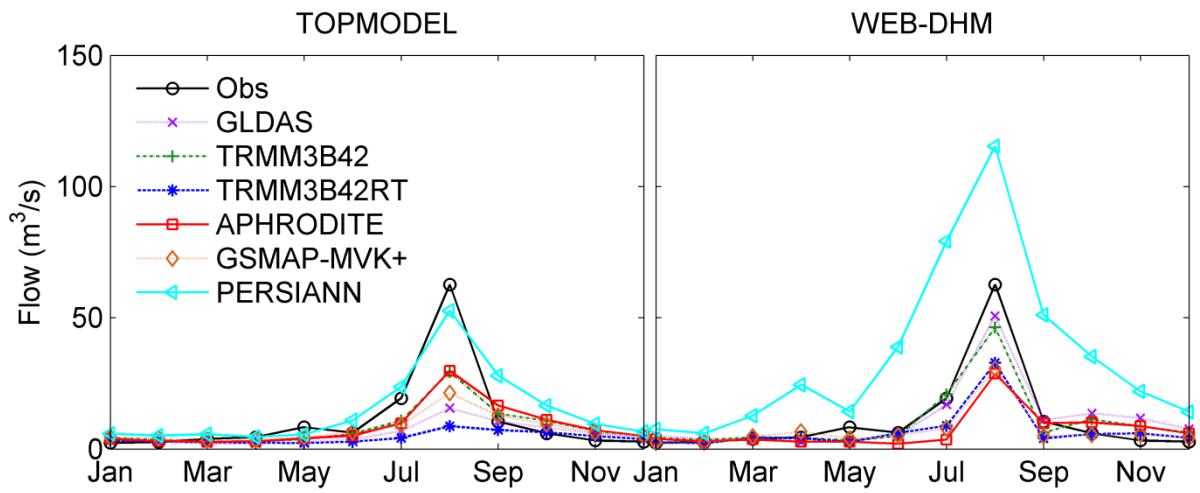
1085



1086

1087 Fig. 13 Scatterplots of simulated discharges with TOPMODEL against gauge observations at  
 1088 a monthly scale.

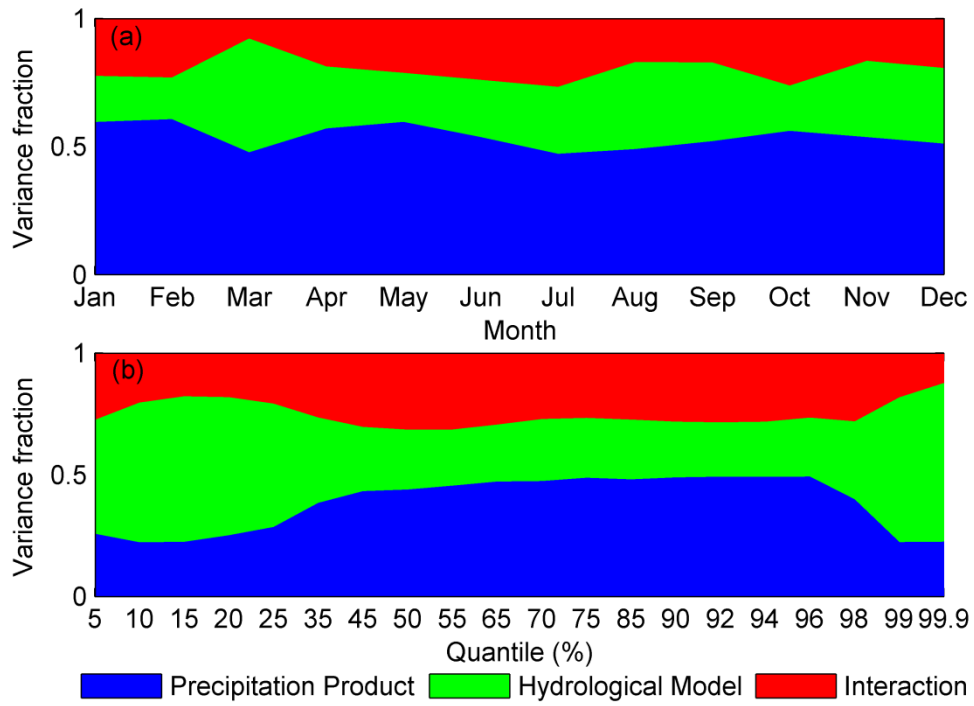
1089



1090

1091 Fig. 14 Inter-annual average monthly discharges.

1092



1093

1094 Fig. 15 Contributions of uncertainty sources to (a) average monthly discharges and (b)

1095 discharge quantiles based on daily scale simulated results.

1096